This is the peer reviewed version of the following article: ***"Puiggalí-Jou, J., del Valle, L.J., Armelin, E., Aleman, C.*** **(2016). Fibrin association at hybrid biointerfaces made of Clot-Binding peptides and polythiophene. Macromolecular bioscience, vol 16 (10), 1461–1474."** *which has been published in final form at* **[doi10.1002/mabi.201600128].** *This article may be used for non-commercial purposes in accordance with Wiley Terms and Conditions for Self-Archiving."*

DOI: 10.1002/marc

Full Paper

Fibrin Association at Hybrid Biointerfaces Made of Clot-Binding Peptides and Polythiophene

Anna Puiggalí,[1,2] Luis J. del Valle,[1,2,*] Elaine Armelin[1,2] and Carlos Alemán[1,2,*]

A. Puiggalí, Dr. L. J. del Valle, Dr. E. Armelin, Prof. Dr. C. Alemán
Departament d'Enginyeria Química, E. T. S. d'Enginyeria Industrial de Barcelona, Universitat Politècnica de Catalunya, Diagonal 647, Barcelona E-08028, Spain.
Centre for Research in Nano-Engineering, Universitat Politècnica de Catalunya, Edifici C', C/Pasqual i Vila s/n, Barcelona E-08028, Spain

E-mail: luis.javier.del.valle@upc.edu and carlos.aleman@upc.edu

Abstract. The properties as biointerfaces of electroactive conducting polymer-peptide biocomposites formed by poly(3,4-ethylenedioxythiophene) (PEDOT) and CREKA or CR(*N*Me)EKA peptide sequences (where Glu has been replaced by *N*-methyl-Glu in the latter) have been compared. CREKA is linear pentapeptide that recognizes clotted plasma proteins and selectively homes to tumors, while CR(*N*Me)EKA was engineer to improve such properties by altering peptide···fibrin interactions. Differences between PEDOT-CREKA and PEDOT-CR(*N*Me)EKA reflect dissemblance in the organization of the peptides into the polymeric matrix. Both peptides affect fibrinogen thrombin–catalyzed polymerization causing the immediate formation of fibrin, whereas in absence of thrombin this phenomenon is only observed for CR(*N*Me)EKA. Consistently, the fibrin-adsorption capacity is higher for PEDOT-CR(*N*Me)EKA than for PEDOT-CREKA, even though in both cases adsorbed fibrin exhibits round-like morphologies rather than the characteristic fibrous structure. PEDOT-peptide films coated with fibrin are selective in terms of cell adhesion, promoting the attachment of metastatic cells with respect to normal cells.

FIGURE FOR ToC_ABSTRACT

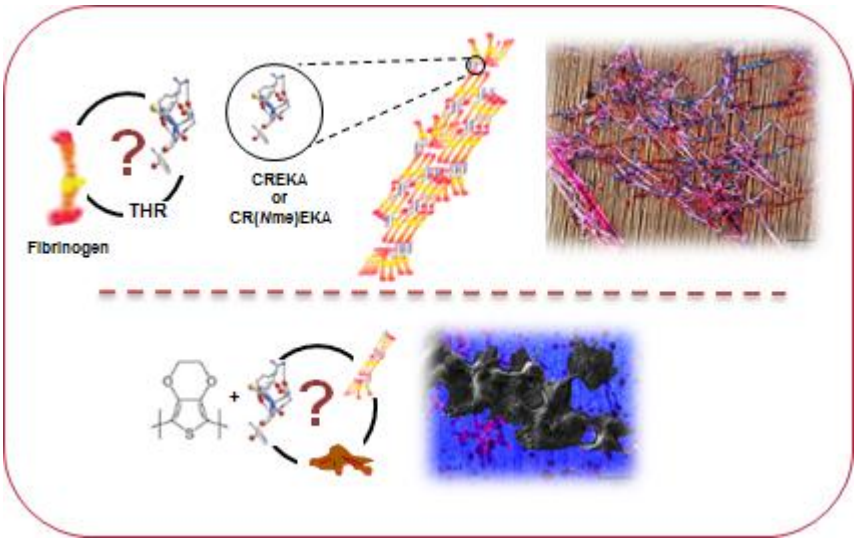

1. Introduction

Biocomposites derived from the conjugation of synthetic polymers with biomolecules (*e.g.* proteins and peptides) are frequently used in biomedicine because of the synergistic effects associated to combination of their individual properties.[1,2] In the last few years, particular attention has been paid to biocomposites involving electroactive conducting polymers (ECPs), which due to their excellent properties[3] are used to fabricate electrochemically active biointerfaces. Thus, devices based on the combination of ECPs and biomolecules have been successfully used applications, as for example bioinspired channels for ion-exchange[4] electromechanical actuators,[5] components of bioelectronics devices,[6] aerogels for nerve regeneration,[7] and bioactive platforms for tissue regeneration that mimic the growth of biological tissues.[8]

CREKA (Cys-Arg-Glu-Lys-Ala) is a linear pentapeptide that recognizes clotted plasma proteins and selectively homes to tumors.[9] Thus, this peptide, which was identified using *in vivo* screening of phage-display peptide libraries,[10] recognizes the interaction of fibrin-fibronectin accumulated in walls of tumor vessels and in the interstitial spaces within tumors.[9] Tumor vessels are less robust and stable than normal vasculature, favoring the release of some molecules such as fibrinogen (Fg), which is the fibrin precursor.[11] Leaked Fg is converted into a fibrin meshwork by the action of thrombin (THR), which cleavages and removes fibrinopeptides allowing the self-assembly of fibrin monomers into elongated fibers.[12] CREKA linked to amino-dextran coated superparamagnetic iron oxide (SPIO) nanoparticles not only binds to clotted plasma proteins blood and plasma but also induces further localized tumor clotting.[9] This amplified system enhanced the homing of the nanoparticles in a mouse tumor model and the tumor imaging, without causing clotting or other obvious side effects elsewhere in the body. CREKA also homes to the surface of atherosclerotic plaques,

including bivalirudin (*i.e.* a THR inhibitor that selectively and reversibly binds the active site of free and fibrin bound THR) containing micelles, and has been used to deliver and concentrate payloads onto atherosclerotic plaques in the ApoE-null mouse model.[13]

The energy landscape and bioactive conformation of CREKA, which consists in a pocket-like shape with the charged groups of Arg, Glu and Lys pointing outwards to facilitate the formation of intermolecular interactions, were determined using computer assisted modelling tools.[14] This information was used to engineer variants of CREKA peptide to resists proteolysis by targeted replacements.[15] More specifically, peptide analogues that incorporate the synthetic α-methyl and *N*-methyl derivatives of Arg, Glu and Lys were studied. Interestingly, CREKA analogues were more effective in tumor homing than the original peptide, results being particularly good for the CREKA analogue in which the Glu was replaced by *N*-methyl-Glu, CR(*N*Me)EKA.[16] Additionally, in a very recent study She et *al.*[17] reported that CR(*N*Me)EKA retains almost completely the anticoagulant activity of the THR inhibitor bivalirudin. In a very recent work we reported the conditions required for the preparation of bioactive platforms based on the modification of an effective ECP with CREKA.[2] The polymer selected for such purpose was poly(3,4-ethylenedioxythiophene) (PEDOT), which is among the most successful ECPs due to its excellent electrochemical and thermal properties, high conductivity, good environmental stability in its doped state, mechanical flexibility, relative ease of preparation, biocompatibility, and fast doping-undoping process.[18] PEDOT-CREKA biocomposites prepared by chronoamperometry in basic aqueous solution (pH= 10.3) and deposited onto a PEDOT internal layer (*i.e.* forming a bilayered system) were found to entrap one peptide molecule every six polymer repeat units. Although the morphology and topography of PEDOT-CREKA

were completely different to those of the individual ECP, the impact of the entrapped peptide molecules in the excellent electrochemical properties of PEDOT was found to be practically negligible. Herein, we prepare and characterize a biocomposite based on the combination of PEDOT and CR(*N*Me)EKA, PEDOT-CR(*N*Me)EKA. This new material has been obtained by adapting the strategy previously used for PEDOT-CREKA[2] to achieve both *(i)* a reduction of an order of magnitude in the thickness of the films, and *(ii)* an improvement of the electrochemical behavior with respect to pure PEDOT. Results indicate that the replacement of Glu by *N*-methyl-Glu affects considerably the biocomposite···fibrin interactions, greatly influencing the properties and response of fibrin-coated biocomposites. Moreover, fibrin-coated PEDOT-CR(*N*Me)EKA exhibits a remarkable capacity to differentiate between normal and tumor cells. Thus, such ECP-peptide-protein biocomposite is a very promising material for biomedical applications.

2. Experimental Section

Materials as well as extended version of the synthetic and characterization protocols are provided in the Supporting Information (S.I.).

2.1. Synthesis

Anodic polymerization and electrochemical assays were performed with an Autolab PGSTAT302N equipped with the ECD module (Ecochimie, the Netherlands) using a three-electrode compartment cell under nitrogen atmosphere (99.995% pure) at room temperature. Steel AISI 316 sheets of 0.5 and 1 cm^2 in area were used as working and counter electrode, respectively. The reference electrode was an Ag|AgCl electrode containing a KCl saturated aqueous solution.

PEDOT-CR(*N*Me)EKA and PEDOT-CREKA films were prepared by chronoamperometry using an aqueous medium pH = 10.3 (adjusted with 1 M NaOH) and a constant potential of 1.10 V using dodecylbenzene sulfonate (SDBS) as supporting electrolyte. Initially, a coating layer of PEDOT was deposited onto the steel electrode using a monomer solution and a polymerization time of θ= 10 s. After this, a second layer of PEDOT-CR(*N*Me)EKA or PEDOT-CREKA was electrodeposited onto the surface of the PEDOT coating layer. This was achieved by including in the anodic compartment a mixture of monomer and CR(*N*Me)EKA or CREKA peptide and using a polymerization time of θ= 20 s. It should be remarked that the biocomposite layer was deposited onto the internal PEDOT layer immediately after the generation of the latter, which represents an important difference with respect to previous work.[2] PEDOT films used as control were prepared employing the same experimental conditions that for PEDOT-peptide biocomposites but without the peptide addition in the second layer.

2.2. Characterization

Film thickness measurements were carried out using a Dektak 150 stylus profilometer (Veeco, Plainview, NY). AFM was conducted to obtain topographic images of the films surface using silicon TAP 150-G probe (Budget Sensors, Bulgaria) with a frequency of 150 kHz and a force constant of 5 N/m. Images were obtained with an AFM Dimension microscope using a NanoScope IV controller under ambient conditions in tapping mode. The scan window size was 10×10 μm^2.

X-ray photoelectron spectroscopy (XPS) analyses were performed in a SPECS system equipped with a high-intensity twin-anode X-ray source XR50 of Mg/Al (1253 eV/1487 eV) operating at 150 W, placed perpendicular to the analyzer axis, and using a Phoibos 150 MCD-9 XP detector. The X-ray spot size was 650 mm. The pass energy

was set to 25 and 0.1 eV for the survey and the narrow scans, respectively. The C 1s peak was used as an internal reference with a binding energy of 284.8 eV.

Cyclic voltammetry (CV) studies were run to assess the electrochemical behavior of the biocomposites. Hence, the ability to exchange charge reversibly (*i.e.* electroactivity) and the electrochemical stability *(i.e.* electrostability) were determined using a 0.1 M phosphate buffer saline solution (PBS; pH= 7.4 adjusted with NaOH). The initial and final potentials were -0.40 V, whereas a reversal potential of 0.80 V was considered. The scan rate was 50 mV/s in all cases. The electrochemical stability (*i.e.* loss of electroactivity, LEA) was determined using the following expression:

$$LEA = \frac{\Delta Q}{Q_i} 100 \qquad (1)$$

where ΔQ is the difference of voltammetric charge between the first cycle and the last cycle and Q_i is the voltammetric charge corresponding to the second cycle.

Real-time monitoring of fibrin polymerization in presence and absence of peptide at 37 ºC was conducted by Dynamic light scattering (DLS) following the increment of the particle effective diameter. Final concentrations of Fg and thrombin (THR) were 0.4 mg/mL and 0.01 U/mL, respectively, in aqueous solution containing 5 mM $CaCl_2$ and 76 mM NaCl. Data were collected every minute. Measurements were performed using a NanoBrook Omni Zeta Potential Analyzer from Brookheaven Instruments Corporation.

Electrochemical impedance spectroscopy (EIS) was performed using a conventional three-electrode cell and AUTOLAB-302N potentiostat/galvanostat operating between the frequency range of 100kHz-10 mHz and 10 mV of amplitude for the sinusoidal voltage. All experiments were performed with films electrochemically deposited on stainless steel substrates (AISI 316L with $1cm^2$ of area) and immersed in phosphate buffer saline (PBS, pH 7.4), at room temperature.

Scanning electron microscopy (SEM) micrographs were obtained using a Focussed Ion Beam Zeiss Neon 40 scanning electron microscope operating at 10 kV. Furthermore, THR-catalyzed fibrin particles were also observed by optical microscopy.

Contact angle (CA) measurements were conducted using the water drop method. 0.5 µL of milliQ water drops were deposited onto the surface of the films and recorded after stabilization with the equipment OCA 15EC (DataPhysics Instruments GmbH, Filderstadt).

2.3. Protein Adsorption

Analyses to examine the adsorption of proteins onto the surface of PEDOT, PEDOT-CREKA and PEDOT-CR(*N*Me)EKA films were performed using fibrin and bovine serum albumin (BSA, Fraction V). BSA, which is a globular plasma protein, was used as a control to study the selectivity of the examined surfaces. The detection of the adsorbed proteins was carried out using the Bradford method. Details about the experimental protocol are provided in the S.I.

2.4. Cell Capture Assays.

Substrates were placed into a 24-well plate, and 1 mL of cell MCF-7 (breast cancer cell line), PNT2 (normal prostate epithelial cell line) or PC-3 (cancer prostate epithelial cell line) suspension (10^5 cells/mL) was loaded. After incubation for 30 min at 37 ºC, 5% CO_2 with slight agitation (80 rpm), the substrates were washed with PBS, located in a new 24-well plate and incubated for 24 hours. The percentage of cells adhered in the substrate with respect to the amount deposited into the well was determined using the MTT [3-(4,5-dimethylthiazol-2-yl)-2,5-diphe- nyltetrazolium] method. Cell capture assays were repeated two times with at least 4 replicas, showing similar results in all

cases. Details about the protocol followed for observation of the cell morphology by SEM are provided in the S.I.

3. Results and Discussion

3.1. PEDOT-Peptide Characterization

The synthetic approach used in this work to prepare PEDOT (control) and PEDOT-peptide bilayered films is summarized in Figure 1. In order to overcome the fragility of PEDOT-peptide films, an internal PEDOT layer was electrodeposited between the steel and the biocomposite. The average thickness (*L*) of the internal PEDOT layer was *L*= 150±35 nm. Bilayered systems containing an external PEDOT, PEDOT-CREKA or PEDOT-CR(*N*Me)EKA layer deposited onto the internal layer exhibited *L* values of 340±72, 573±57 or 498±35 nm, respectively. These *L* values, which were achieved by depositing the external layer immediately after polymerize the internal PEDOT layer, are considerably smaller than those reported in for bilayered PEDOT-CREKA (*L*= 3.8±1.3 μm).[2] Thus, in the latter case the apparition of multiple, prominent, and well-localized folds homogeneously distributed was promoted by drying during several hours the internal layer before the deposition of the external layer.[2] Accordingly, elimination of the drying process induces significant changes not only in *L* but also on the properties (see below) despite the experimental conditions used for the anodic polymerization are practically identical.

Comparison of the root mean square roughness (Rq) determined by AFM for the external layer of PEDOT, PEDOT-CREKA or PEDOT-CR(*N*Me)EKA (Rq= 74±9, 133±23 and 161±11 nm, respectively) indicates that the peptide affects the surface topography (Figure 2). PEDOT's surface can be described as a very homogeneous distribution of small molecular aggregates, which has been associated with the linear

growing of polymer chains.[19] Incorporation of CR(*N*Me)EKA or CREKA into the polymeric matrix provokes a drastic change in the topography that exhibits high and relatively large compact blocks, explaining the enhancement of Rq. These blocks, which result from the aggregation of small clusters over the polymer surface, are essentially induced by the role of the peptide as doping agent. Thus, peptide molecules (individually or forming clusters) embedded into the PEDOT matrix alter the growing of polymer chains, which should perpendicular to the electrode surface. As PEDOT chains tend to grow forming clusters,[20] the tilting induced by the peptide facilitates the aggregation of neighboring clusters. These phenomena are more pronounced for PEDOT-CR(*N*Me)EKA than for PEDOT-CREKA.

PEDOT and PEDOT-peptide composites were characterized by XPS. The atomic percent composition (C 1s, N 1s, O 1s and S 2p) of the three systems are compared in Table 1. As it can be seen, nitrogen was detected in the composition of the three systems. According to the experimental conditions used in this work, the penetration of X-ray radiation is expected to be of ~10 nm. Although the thickness of the bilayered films prepared in this work ranged from ~300 to ~600 nm, examination by SEM revealed some uncoated regions of the steel substrate. Accordingly, the presence of N 1s in PEDOT films has been attributed to the metallic substrate.[21] It is worth noting that the N 1s content increases from 0.47% in PEDOT to 1.20% and 0.92% in PEDOT-CREKA and PEDOT-CR(*N*Me)EKA, respectively, reflecting the successful incorporation of the peptides.

Assuming that the nitrogen coming from the steel substrate is approximately the same for the three systems, the number of polymer repeat units per peptide molecule in PEDOT-CREKA and PEDOT-CR(*N*Me)EKA can be roughly estimated using the $S/(N_p–N_s)$ ratio (Table 1), where S is the total percent composition of sulfur atoms and

(N_p–N_s) refers to the difference between the total percent composition of nitrogen at PEDOT-peptide and PEDOT. According to this approximation, the content of peptide in PEDOT-CREKA and PEDOT-CR(*N*Me)EKA is relatively high with one peptide molecule every ~10 and ~15 polymer repeat units, respectively. The smaller content of immobilized peptide molecules in PEDOT-CR(*N*Me)EKA is due to the increment of the molecular volume provoked by the *N*-methylation of the Glu residue, which enhanced peptide–polymer steric interactions during the polymerization process.

Figure 3 displays the high-resolution XPS spectra in the N 1s region, which is crucial to prove the immobilization of the peptide into the ECP matrix, for PEDOT, PEDOT-CREKA and PEDOT-CR(*N*Me)EKA. The peak centered around 402 eV, which was detected in all examined samples including PEDOT ones, is consequence of impurities of the AISI 316 steel (see above).[21] However, the intense peak found at 400.2 eV for both PEDOT-CREKA and PEDOT-CR(*N*Me)EKA corresponds to the peptides. Thus, this peak is typically explained as a combination of the guanidinium (400.1 eV) and the backbone amide (400.5 eV) signals.[22] Bhattacharyya and Gleason attributed the presence of N 1s characteristic peaks at 399.7 eV (–NH) and 400.4 eV (N–C=O) to bovine serum albumin attached to the surface of a copolymer of thiophene-3-acetic acid and EDOT.[23] Similarly, the XPS N–H signal of Boc-Val-Gly-Gly-Val-Gly-OEt and poly(Val-Gly-Gly-Val-Gly) were identified at 400.0 and 400.2 eV, respectively.[24]

Electrochemical properties of PEDOT improve upon the incorporation of the peptide, independently of the chemical modification at the Glu residue. Figure 4a shows that the electroactivity of both PEDOT-peptide systems is around 15% higher than that of PEDOT. These results are consistent with the role of CREKA and CR(*N*Me)EKA molecules as dopant ions, participating in oxidation and reduction processes. This achievement, which is in marked contrast previous results,[2] is due to the elimination of

the drying step before the deposition of the external layer. The presence of the peptide also enhances the electrochemical stability of PEDOT, as is reflected by the control voltammograms recorded after five consecutive oxidation-reduction cycles in PBS (Figure 4b). After such amount of cycles, the electroactivity of PEDOT is lower than that of PEDOT-CREKA and PEDOT-CR(*N*Me)EKA by 20% and 30%, respectively. Analysis of the LEA (Equation 1) shows a reduction of ~15% and 25% for PEDOT-peptide and PEDOT, respectively, after 5 redox cycles (Figure 4c).

The reduction of the electroactivity with the number of redox cycles is related with the structural degradation of the polymeric matrix that becomes less porous (*i.e.* more compact), making difficult the escape and entrance of dopant ions during the oxidation and reduction processes, respectively. In the case of PEDOT-CREKA and PEDOT-CR(*N*Me)EKA, the peptides impart protection to the matrix preventing its structural degradation. Although determination of such protection mechanism is not an easy task, our hypothesis is based on a steric protection due to the formation of nanometric and insoluble peptide aggregates inside the polymeric matrix. These could act as structural support avoiding the collapse of the polymeric matrix and maintaining the porosity.

3.2. Influence of the Peptide in Fibrinogen Polymerization

In order to mimic the extracellular conditions where CR(*N*M*e*)EKA is able to selectively bind into tumor regions, the affinity of the this peptide towards fibrin has been compared with that CREKA. The formation of fibrin networks is the central event in vertebrates blood coagulation[25,26] and is involved in several pathologies like thrombosis and cancer metastasis.[26,27] From a physiological point of view, it represents the end of the coagulation cascade when THR activates the inactive precursor Fg.[26,28] Cleavage and removal of fibrinopeptides from Fg by THR promote the interaction

between neighboring fibrin molecules that self-associate to form elongated fibers and fiber networks.[12,29]

The effect of the peptides on fibrin THR-catalyzed polymerization was assessed at 37 ºC by DLS. Figure 5 represents the temporal evolution of the effective diameter (D_{eff}) of Fg particles using conditions optimized to examine the early steps in fibrin polymerization[30] (*i.e.* 0.4 mg/mL Fg aqueous solution containing 5 mM $CaCl_2$ and 76 mM NaCl). In absence of THR, D_{eff} stabilizes at ~32 nm (Figure 5a) indicating significant restrictions in association process (*i.e.* hydrodynamic radius of Fg is ~13 nm[31]). Instead, D_{eff} grows rapidly and progressively over time upon the incorporation of THR (Figure 5a). The value of D_{eff} reaches a plateau after 55 min at approximately 2.5 μm, which corresponds to the THR-induced fibrin polymerization.[12]

The influence of CREKA and CR(*N*Me)KA in fibrin polymerization was studied by adding each peptide to Fg aqueous solutions with and without THR (Figure 5b and 5c). In absence of enzyme, the increase of D_{eff} reflects that the two peptides promote the aggregation of Fg, even though quantitative differences in the aggregation mechanism are revealed. CREKA induces a sustained linear increase of D_{eff}, which grows from ~45 nm (t= 1 min) to ~191 nm (t= 60 min). In contrast, CR(*N*Me)EKA provokes a very fast aggregation process at the initial stage ($D_{eff}\approx$ 380 nm at t= 1 min), the growing of the microparticles remaining practically stopped after this event ($D_{eff}\approx$ 347 nm at t= 60 min). Interestingly, incorporation of the peptides to the Fg solution in presence of THR results in very fast aggregation process. Thus, the D_{eff} value of the particles formed at t= 1 min is ~271 and ~574 nm for CREKA and CR(*N*Me)EKA, respectively. After this initial stage, the size of particles progressively increased, even though the peptide largely influenced the growth rate. In the case of CREKA the growth rate of the particles (6.9±0.3 nm/min from Figure 5b) decreased considerably with respect to the

same solution without peptide (50.5±1.8 nm/min from Figure 5a). After a liner growth regime, D_{eff} stabilized around ~712 nm, which represents a reduction of around 72 % with respect to the value obtained for the same solution but without CREKA. After a very fast formation stage, the growth rate of the particles formed in presence of CR(*N*Me)EKA progressively increases (14.1±0.3 nm/min from Figure 5c), stabilizing at D_{eff}≈ 1343 nm after 55 min. Accordingly, both peptides disturb the THR-induced fibrin polymerization, even though such effect is significantly more pronounced for CREKA.

In an early work, Carr *et al*.[32] proved that positively charged poly(α-amino acid)s enhance lateral association of fibrin protofibrils during fiber bundling. This phenomenon was attributed to the charge and isoelectric point of such polypeptides. High pKa values facilitated strong interaction between the protofibrils and the poly(α-amino acid), independently of the molecular weight, promoting fibrin polymerization, as was evidenced by the increase of fibrin fibers diameter.[32] In contrast, no effect was observed for negatively charged poly(α-amino acid)s. Both CREKA and CR(*N*Me)EKA have an isoelectric point of 8.55 and, therefore, they are positively charged at working pH (7.4). Accordingly, such peptides could promote the lateral assembly of fibrin protofibrils, reducing the elongation capability of fibers, as suggested in Figure 5.

3.3. Adsorption of Fibrin onto PEDOT-Peptide Films

The selective adsorption of fibrin by PEDOT-peptide biocomposites has been examined by comparing with the adsorption of BSA, which is a globular plasma protein. Results indicate that the affinity of PEDOT-CREKA and PEDOT-CR(*N*Me)EKA toward fibrin fibers was ~2.5 and ~6 times higher than that of PEDOT (Figure S1), respectively. Thus, ~6%, ~14% and ~37% of the fibrin from the initial solution was adsorbed onto PEDOT, PEDOT-CREKA and PEDOT-CR(*N*Me)EKA,

respectively. In contrast, the adsorbed BSA was very scarce (*i.e.* ~8% for PEDOT-CR(*N*Me)EKA and lower than 2% for PEDOT and PEDOT-CREKA). The selectivity of PEDOT-CR(*N*Me)EKA towards fibrin suggests that the distribution of the charged groups in this biocomposite is appropriated for the adsorption of fibrin despite the loss of its fibrous structure (see below). However, such distribution is much less suitable for the adsorption of globular proteins, like BSA, in which polar groups are expected to be randomly distributed.

The morphology of fibrin adsorbed onto PEDOT-peptide films was studied by SEM (Figure 6). For this purpose, the THR-catalyzed polymerization of Fg was stopped after 60 min by the addition of formaldehyde[30] (2.5%) and, subsequently, dehydrated using 30%, 40%, 70%, 90% and 100% ethanol solutions. Amazingly, the formaldehyde-fixed fibrin onto PEDOT-peptide surfaces does not exhibit the expected mesh of fibers (see below)[32,33] but forms agglomerates of micrometric dimensions with very varied morphologies. Thus, agglomerates of fibrin adsorbed onto PEDOT-CREKA (Figure 6a) were relatively small (1-4 μm) and displayed different round-like morphologies, including the spherical one. In contrast, fibrin adsorbed onto PEDOT-CR(*N*Me)EKA presents a larger variety of morphologies, including fiber-like, round-like and completely irregular ones (Figure 6b). As the elongated fiber-like morphologies were relatively infrequent and isolated rather than immersed into a mesh, they have been related with structures formed without the participation of the peptide. Furthermore, fibrin aggregates adsorbed onto PEDOT-CR(*N*Me)EKA are typically bigger than those deposited onto PEDOT-CREKA. Overall, results suggest that the round-like and irregular morphologies of fibrin adsorbed onto PEDOT-peptide are controlled by the fast aggregation processes occurring at early stages of the polymerization process, which is consistent with the DLS observations (Figure 5). The area and aspect ratio

(AR), which is defined by the ratio between length and diameter, of the morphologies observed for the 60 min formaldehyde-fixed products, were determined with the ImageJ software using SEM micrographs. Results indicate that the distribution of both areas and AR (Figure S2) are influenced by the peptide. Thus, 6% of structures formed onto PEDOT-CR(*N*Me)KA shows an area higher than 10 μm^2, such amount being imperceptible for PEDOT-CREKA. Moreover, 8.8% and 20.3% of the structures formed onto PEDOT-CREKA and PEDOT-CR(*N*Me)KA, respectively, exhibit an AR > 2.0, reflecting the sporadic formation of isolated fibril-like structures in the latter (Figure 6b).

In order to further confirm the presence of fibrin onto PEDOT-peptide surfaces, the two biocomposites together with steel and PEDOT were stained with eosin. Figure 7 compares optical microscopy images of red colored fibrin polymerized with THR during 60 min. Although fibrin is apparently able to bind all tested surfaces, differences in the amount of adsorbed proteins indicate a certain degree of selectivity. Thus, a typical intertwined mesh of long fibers oriented in multiple directions is observed when fibrin is deposited onto bare steel (Figure 7a). PEDOT affects drastically the fibrin morphology, inducing the formation of small and rounded-like agglomerates after 60 min (Figure 7b). The abundance of these aggregates is very scarce in comparison to those adsorbed onto steel, which is fully consistent with Bradford protein assays (Figure S1). Thus, the adsorption and morphology of fibrin is largely influenced by the roughness and/or chemical nature of the substrate. Dolatshahi-Pirouz *et al.*[33] showed that fibrin polymerization and, therefore, fibrillation are slower on flat than on rough surfaces. Nevertheless, steel (Rq= 5±2 nm) is flatter than bilayered PEDOT films (Rq= 74±9 nm), evidencing that the chemical nature of the surface is also regulating fibrin polymerization and morphology. The chemical nature influence is apparently reflected

by the surface hydrophilicity, which is considerably higher for PEDOT and PEDOT-peptide than for steel (Table 2).

The hydrophilicity of PEDOT-peptide is similar to that of PEDOT (Table 2), even though the roughness is higher for the formers (Rq= 133±23 and 161±11 nm for PEDOT-CREKA and PEDOT-CR(*N*Me)EKA, respectively) than for the latter (Rq= 74±9 nm). Microscopy images displayed in Figure 7b-7d indicate that the fibrin polymerization rate onto PEDOT-containing surfaces increases with the roughness, which is in agreement with the findings of Dolatshahi-Pirouz *et al.*[33] Thus, the amount of adsorbed fibril increases as follows: PEDOT < PEDOT-CREKA < PEDOT-CR(*N*Me)EKA.

Comparison between the CAs for the different surfaces without and with adsorbed fibrin reveals differences in the wettability (Table 2), especially for PEDOT and PEDOT-peptide systems. Thus, the highly hydrophilic character of such CP and its two biocomposites (CA < 20º) transforms into hydrophobic (CA > 90º) upon the adsorption of fibrin particles. This effect is much less pronounced for steel. The transformation of Fg into fibrin was reported to be accompanied by a change in the wettability from very hydrophilic (Fg) to moderately but definitely hydrophobic (fibrin).[34]

3.4. Influence of Fibrin in PEDOT-Peptide Electrochemical and Electrical Properties

Control voltammograms of PEDOT and PEDOT-peptide films coated with fibrin are displayed in Figure S3. Comparison with those reported in Figure 4a indicates that the adsorbed protein affects negatively the electrochemical response of both the ECP and the biocomposites. More specifically, the adsorption of fibrin reduces the electroactivity of PEDOT, PEDOT-CREKA and PEDOT-CR(*N*Me)EKA by 35%, 50% and 51%,

respectively. The adsorbed protein also affects negatively to the electrochemical stability of the two biocomposites. Thus, after only 5 consecutive redox cycles, the LEA is 18%, 22% and 25% for PEDOT, PEDOT-CREKA and PEDOT-CR(*N*Me)EKA, respectively. Accordingly, the behavior of the biocomposites relative to the ECP is in terms of electrostability the opposite that the one displayed in absence of fibrin (Figure 4b). These results should be attributed to the combination of two related effects: *(i)* the amount of protein at the surface of the biocomposites is considerably higher than at the surface of PEDOT; and *(ii)* protein aggregates are more compact than polymeric and biocomposite matrices. Accordingly, the exchange of ions between the matrix and the PBS electrolytic medium during redox processes is more difficult at regions covered by the protein, which are more abundant at the biocomposites than at PEDOT.

A similar behaviour was observed by EIS analyses. The electrode impedance is related to the interfacial surface area between the electrode and electrolyte. The bare metal only exhibits a low double layer capacitance (CPE_{dl}) and a high polarization resistance coming from the interaction between the ions of the electrolytic medium (PBS) and the heterogeneous steel surface (R_p) (Figure 8a). On the other hand, the impedance of the electrodes covered with a semiconducting material is more complex and other time constants can appear due to several interfaces. More specifically, the impedance of PEDOT-coated electrodes decreases three orders of magnitude with respect to the bare metal across frequencies between 0.01–10 Hz, which correspond to the zone of the coating resistance. This must be attributed, at least partially, to an increase in the effective surface area, which is provided by the porous PEDOT electrode. The coating resistance (R_c), which is identified from the first diameter of the semicircle in the Nyquist plots (Figure S4), describes the resistance for transferring the electrons from the PBS ions to the conducting polymer film.

The diffusion of ions across the films is enhanced upon the incorporation of peptide to PEDOT, leading to lower R_c values (Table 3). The R_c of fibrin-coated PEDOT-peptide films is higher than that of biocomposites without fibrin (Table 3) since the protein aggregates block the pores (*i.e.* barrier effect). This behaviour is more pronounced for PEDOT-CR(*N*Me)KA, supporting that fibrin interacts more favourably with CR(*N*Me)KA than with CREKA. Furthermore, another constant phase element (CPE_{dif} , with n= 0.90) is required to model the response of PEDOT-CR(*N*Me)KA with fibrin (Figure 8b). This is probably due to favourable fibrin⋯peptide interactions, which cause a slow diffusion of ions at very low frequency range. The best-fit values for the adjusted resistances and capacitances are listed in Table 3.

3.5. Cell Capture Selectivity: Tumor versus Normal Cells

PEDOT and PEDOT-peptide samples have been used to investigate the effect of fibrin adsorption on cell capturing with MCF-7 cells (breast cancer cell line). Results, which are displayed in Figure 9a, clearly indicate that MCF-7 cells are captured more efficiently by the biocomposites than by PEDOT. Moreover, the highest cell viability was obtained for PEDOT-CR(*N*Me)EKA coated with fibrin evidencing that such ECP-peptide-protein biocomposite is a very promising material for biomedical applications. Representative SEM micrographs of cells adhered to PEDOT-CR(*N*Me)EKA without and with fibrin are displayed in Figures 9b and 9c, respectively.

On the other hand, the ability of PEDOT-peptide biocomposites to differentiate between tumor and normal cells was examined by conducting cell attachment assays using normal (PNT2) and metastatic (PC-3) prostate epithelial cell lines. Results displayed in Figure 9d indicate that the amount of normal and tumor attached cells is practically the same for the two uncoated biocomposites, no clear preference being

exhibited. Moreover, the influence of the peptide is practically negligible since the cell attachment was practically the same for PEDOT and PEDOT-peptide films. However, assays considering biocomposite films coated with fibrin reveal not only an enhancement of cell attachment but also of cell identification (Figure 9d), *i.e.* normal cells *vs* tumor cells. Thus, both PEDOT-CREKA and PEDOT-CR(*N*Me)EKA films with adsorbed fibrin promoted the adhesion of tumor cells with respect to normal cells by around 12%. Moreover, the capture of PNT2 cells is slightly less efficient for biocomposites with adsorbed fibrin than without such protein. Overall results suggest that cell capture selectivity depends on a balance between different factors, which include surface roughness and morphology in addition to chemical structure.

SEM micrographs of PC3 cells adhered onto fibrin-coated PEDOT-CR(*N*Me)EKA and non-coated PEDOT films are displayed in Figures 9e and 9f, respectively. The former ECP-peptide-protein composite promotes cell attachment, as is clearly reflected by both the formation of multiple inter-cell connections and a very homogeneous spreading of the adhered cells. These features are less evident in Figure 9f, which exhibits not only a lower number of cells but also much less connections among them.

4. Conclusions

PEDOT-peptide biocomposites have been prepared by chronoamperometry in basic aqueous solution. The electrochemical and electrical response of the resulting biocomposites is significantly better than that of the ECP in terms of electroactivity, electrostability and electrical conductivity. Such improvement suggests that peptide molecules play simultaneously two roles acting, on one side, as dopant agents that participate actively in oxidation and reduction processes and, on the other side, as structural supports that preclude the degradation of the ECP during redox processes.

The replacement of Glu by *N*Me-Glu in the peptide alters the surface topology of the biocomposite, entrapped CR(*N*Me)EKA forming bigger aggregates than CREKA.

Both CREKA and CR(*N*Me)EKA affect the fibrin THR-catalyzed polymerization inducing a very fast aggregation process. However, in absence of catalytic enzyme such fast aggregation phenomenon is only promoted by CR(*N*Me)KA, whereas CREKA induces a stepwise linear grow of fibrin particles. This behavior is fully consistent with the ability of the different materials to adsorb fibrin at the surface, which grows in the following way: PEDOT < PEDOT-CREKA < PEDOT-CR(*N*Me)EKA. The two PEDOT-peptide biocomposites, which adsorb selectively fibrin, transform the shape of the adsorbed protein from the typical mesh of fibers to agglomerates with different round-like morphologies. This remarkable change has been attributed to the fact that the morphology of fibrin adsorbed onto the biocomposites is kinetically controlled through the very rapid aggregation process detected at the early stages of the Fg polymerization.

Cell adhesion assays have evidenced that PEDOT-peptide-fibrin films promote the attachment of metastatic cells with respect to that of normal cells. However, this clearly manifested selectivity towards tumor cells is lost in absence of the fibrin coating. The overall of the results obtained in this work for PEDOT-CR(*N*Me)EKA films are currently used to develop new biomedical applications based on hollow nano- and microspheres of such biocomposite.

Supporting Information

Supporting Information is available from the Wiley Online Library or from the author.

Acknowledgements: This work was supported by MINECO-FEDER (MAT2015-69367-R). Support for the research of C.A. was received through the prize "ICREA Academia" for excellence in research funded by the Generalitat de Catalunya.

Keywords: cell differentiation; electroactive polymers; fibrin adsorption; peptide-polymer composites; poly(3,4-ethylenedioxythiophene)

[1] a) F. Han, X. Qi, L. Li, L. Bu, Y. Fu, Q. Xie, M. Guo, Y. Li, Y. Ying, S. Yao, *Adv. Funct. Mater.* **2014**, *24*, 5011; b) C. K. Wong, A. J. Laos, A. H. Sorivadi, J. Wiedenmann, P. M. G. Curmi, J. J. Gooding, C. P. Marquis, M. H. Stenzel, P. Thordarson, *Angew. Chem. Int. Ed.* **2015**, *54*, 5317; c) Y. Z. Wu, D. Y. W. Ng, S. L. Kuan, T. Weil, *Biomat. Sci.* **2015**, *3*, 214; d) S. T. Gunawan, K. Kempe, G. K. Such, J. W. Cui, K. Liang, J. J. Richardson, A. P. R. Johnston, *Biomacromolecules* **2014**, *15*, 4429; e) B. Guo, L. Glavas, C. A. Albertsson, *Prog Polym Sci*. **2013**, *38*,1263.

[2] G. Fabregat, B. Teixeira-Dias, L. J. del Valle, E. Armelin, F. Estrany, C. Alemán, *Appl. Mater. Interfaces* **2014**, *6*, 11940.

[3] a) C. Li, H. Bai, G. Shi, *Chem. Soc. Rev.* **2009**, *38*, 2397; c) E. C. S. Coelho, V. B. Nascirnento, A. S. Ribeiro, M. Navarro, *Electrochim. Acta* **2014**, *123*, 441; b) Y.-Z. Longa, M.-M. Lia, C. Gub, M. Wanc, J.-L. Duvaild, Z. Liue, Z. Fanf, *Prog. Polym. Sci.* **2011**, *36*, 1415.

[4] M. M. Pérez-Madrigal, L. J. del Valle, E. Armelin, C. Michaux, G. Roussel, E. A. Perpetè, C. Alemán, *ACS Appl. Mater. Interfaces* **2015**, *7*, 1632.

[5] I. S. Romero, N. P. Bradshaw, J. D. Larson, S. Y. Severt, S. J. Roberts, M. L. Schiller, J. M. Leger, A. R. Murphy, *Adv. Funct. Mater*. **2014**, *24*, 3866.

[6] a) M. Hamedi, J. Wigenius, F.-I. Tai, P. Björk, D. Aili, *Nanoscale*, **2010**, *2*, 2058; b) D. E. López-Pérez, D. Aradilla, L. J. del Valle, C. Alemán, *J. Phys. Chem. C* **2013**, *117*, 6607.

[7] Z. Q. Shi, H. C. Gao, J. Feng, B. B. Ding, X. D. Cao, S. Kuga, Y. J. Wang, L. N. Zhang, J. Caj, *Angew. Chem. Int. Ed.* **2014**, *53*, 5380.

[8] a) J. Soto-Delgado, J. Torras, L. J. del Valle, F. Estrany, C. Alemán, *RSC Adv.*, **2015**, *5*, 9189; (b) M. M. Pérez-Madrigal, M. I. Giannotti, L. J. del Valle, L. Franco, E. Armelin, J. Puiggalí, F. Sanz, C. Alemán, *ACS Appl. Mater. Interfaces*, **2014**, 6, 9719-9732.

[9] D. Simberg, T. Duza, J. H. Park, M. Essler, J. Pilch, L. Zhang, A. M. Derfus, M. Yang, R. M. Hoffman, S. Bathia, M. J. Sailor, E. Ruoslahti, *Proc. Natl. Acad. Sci. U.S.A.* **2007**, *104*, 932.

[10] a) R. Pasqualini, E. Ruoslahti, *Nature* **1996**, *380*, 364; b) J. A. Hoffman, E. Giraudo, M. Singh, L. Zhang, M. Inoue, K. Porkka, D. Hanahan, E. Ruoslahti, *Cancer Cell* **2003**, *4*, 383.

[11] F. Yuan, M. Dellian, D. Fukumura, M. Leunig, *Cancer Res.* **1995**, *55*, 3752.

[12] E. T. O'Brien III, M. R. Falvo, D. Millard, B. Eastwood, R. M. Taylor II, R. Superfine, *Proc. Natl. Acad. Sci.* **2008**, *105*, 19438.

[13] a) D. Peters, M. Kastantin, V. R. Kotamraju, P. P. Karmali, K. Gujraty, M. Tirrell, E. Ruoslahti, *Proc. Natl. Acad. Sci. U.S.A.* **2009**, *106*, 9815; b) J. Hamzah, V. R. Kotamraju, J. W. Seo, L. Agemy, V. Fogal, L. M. Mahakian, D. Peters, L. Roth, M. K. Gagnon, K. W. Ferrara, E. Ruoslahti, *Proc. Natl. Acad. Sci. U.S.A.* **2011**, *108*, 7154.

[14] a) D. Zanuy, A. Flores-Ortega, J. Casanovas, D. Curco, R. Nussinov, C. Alemán, *J Phys Chem B* **2008**, *112*, 8692; b) D. Zanuy, D. Curcó, R. Nussinov, C. Alemán, *Biopolymers (Pept Sci)* **2009**, *92*, 83.

[15] D. Zanuy, F. J. Sayago, G. Revilla-López, G. Ballano, L. Agemy, V. R. Kotamraju, A. I. Jiménez, C. Cativiela, R. Nussinov, A. M. Sawvel, G. Stucky, E. Ruoslahti, C. Alemán, *J. Comput. Aided. Mol. Des.* **2013**, *27*, 31.

[16] L. Agemy, K. N. Sugahara, V. R. Kotamraju, K. Gujraty, O. M. Girard, Y. Kono, R. F. Mattrey, J.-H. Park, M. J. Sailor, A. I. Jimenez, C. Cativiela, D. Zanuy, F. J. Sayago, C. Alemán, R. Nussinov, E. Ruoslahti, *Blood* **2010**, *116*, 2847.

[17] Z.-G. She, X. Liu, V. R. Kotamraju, E. Ruslahti, *ACS Nano* **2014**, *8*, 10139.

[18] a) L. Groenendaal, G. Zotti, P.-H. Aubert, S. M. Waybright, J. R. Reynolds, *Adv. Mater.* **2003**, *15*, 855; b) L. Groenendaal, F. Jonas, D. Freitag, H. Pielartzik, J. R. Reynolds, *Adv. Mater.* **2000**, *12*, 481; c) S. Kirchmeyer, K. Reuter, *J. Mater. Chem*, **2005**, *15*, 2077; d) L. J. del Valle, F. Estrany, E. Armelin, R. Oliver, C. Alemán, *Macromol. Biosci.* **2008**, *8*, 1144.

[19] D. Aradilla, D. S. Azambuja, F. Estrany, M. T. Casas, C. A. Ferreira and C. Alemán, *J. Mater. Chem.* **2012**, *22*, 13110.

[20] D. Zanuy and C. Alemán, *Soft Matter* **2014**, *9*, 11634.

[21] a) G. Fabregat, G. Ballano, E. Armelin, L. J. del Valle, C. Cativiela and C. Alemán, *Polym. Chem*. **2012**, *4*, 1412; b) S. Maione, A. M. Gil, G. Fabregat, L. J. del Valle, J. Triguero, A. Laurent, D. Jacquemin, F. Estrany, A. I. Jiménez, D. Zanuy, C. Cativiela and C. Alemán, *Biomat. Sci.* **2015**, *3*,1395.

[22] J. S. Stevens, A. C. de Luca, M. Pelendritis, G. Terenghi, S. Downes and S. L. M. Schroeder, *Surf. Interface Anal.* **2013**, *45*, 1238.

[23] D. Bhattacharyya and K. K. Gleason, *Chem. Mater*. **2011**, *23*, 2600.

[24] R. Flamia, G. Lanza, A. M. Salvi, J. E. Castle and A. M. Tamburro, *Biomacromolecules* **2005**, *6*, 1299.

[40] R. F: Doolittle, *The molecular biology of fibrin*, in *The Molecular Basis of Blood Diseases* (Eds: G. Stamatoyannopoulos, P. W. Majerus, R. M. Perlmutter and H. Varmus), Saunders, Philadelphia **2000**, pp 719-739.

[26] B. Blombäk, *Thromb. Res*. **1996**, *83*, 1.

[27] C. Boccaccio and E. Medico, *Cell. Mol. Life Sci*. **2006**, *63*, 1024.

[28] a) R. F. Doolittle, *Annu. Rev. Biochem*. **1984**, *53*, 195; b) J. W. Weisel, *Adv. Protein Chem*. **2005**, *70*, 247.

[29] J. W. Weisel, *J Thromb Haemost* **2007**, *5*, 116.

[30] L. Huang, J. P.-L. Hsiao, C. Powierza, R. M. Taylor II and S. T. Lord, *Biochemistry* **2014**, *53*, 7824.

[31] a) M. Wasilewska, Z. Adamczyk and B. Jachimska, *Langmuir* **2009**, *25*, 3698; b) E. G. Zavyalova, A. D. Protopopova, A. M. Kopylov and I. V. Yaminsky, *Langmuir* **2011**, *27*, 4922.

[32] M. E. Carr Jr., R. Cromartie and D. A. Gabriel, *Biochemistry* **1989**, *28*, 1384.

[33] A. Dolatshahi-Pirouz, M. Foss and F. Besenbacher, *J. Phys. Chem. C* **2011**, *115*, 13617.

[34] C. J. van Oss, *J Protein Chem.* **1990**, *9*, 487.

Table 1. Atomic percent composition (C 1s, N 1s, O 1s and S 2p) and S 2p / N 1s ratio obtained by XPS for PEDOT, PEDOT-CREKA and PEDOT-CR(*N*Me)EKA.

#	C 1s	N 1s	O 1s	S 2p	S / N
PEDOT	68.64	0.47	23.82	7.07	-
PEDOT-CREKA	68.57	1.20	23.06	7.17	5.97
PEDOT-CR(*N*Me)EKA	69.46	0.92	22.74	6.88	7.48

Table 2. Contact angle (CA) determined for the surfaces examined in this work before and after adsorption of fibrin.

Surface	**CA**
Steel	68º±5º
PEDOT	< 20º
PEDOT-CREKA	< 20º
PEDOT-CR(*N*Me)EKA	< 20º
Steel / fibrin	94º±4º
PEDOT / fibrin	112º±1º
PEDOT-CREKA / fibrin	114º±2º
PEDOT-CR(*N*Me)EKA / fibrin	107º±4º

Table 3. Resistances (R) and constant phase elements (CPE) for each sample analysed with EIS technique and after adjusting the parameters using the electrical equivalent circuit (EEC) shown in Figure 8b.

Sample	R_s [a] ($\Omega.cm^2$)	R_c [b] ($\Omega.cm^2$)	CPE_c [c] ($F\ cm^{-2}\ s^{n-1}$)	n	R_p [d] ($\Omega.cm^2$)	CPE_{dl} [e] ($F\ cm^{-2}\ s^{n-1}$)	n	CPE_{dif} [f] ($F\ cm^{-2}\ s^{n-1}$)	n
Stainless steel (bare)	123	-	-	-	594k[g]	3.85×10^{-5}	0.85	-	-
PEDOT	162	267	4.03×10^{-5}	0.83	-	1.08×10^{-3}	0.76	-	-
PEDOT-CREKA	100	188	1.00×10^{-4}	0.74	-	1.12×10^{-3}	0.93	-	-
PEDOT-CREKA with fibrin	155	209	3.49×10^{-5}	0.73	-	1.23×10^{-3}	0.91	-	-
PEDOT-CR(*N*Me)EKA	119	128	2.29×10^{-4}	0.54	-	0.82×10^{-3}	1.00	-	-
PEDOT-CR(*N*Me)EKA with fibrin	97	294	6.30×10^{-4}	0.63	138[h]	0.87×10^{-3}	1.00	2.25×10^{-4}	0.90

[a] R_s = solution resistance, [b] R_c = Coating resistance, [c] CPE_c = coating capacitance, [d] R_p = polarization resistance, [e] CPE_{dl} = double layer capacitance [f] CPE_{dif} = diffusion capacitance, [g] Value of resistance for the stainless steel bare (without conducting polymer) is attributed to the polarization resistance (R_p) in the electrode/electrolyte interface at low frequency. [h] This parameter is better related to the R_{dif} = ion diffusion resistance across the film (see the last EEC in Figure 8b).

CAPTIONS TO FIGURES

Figure 1. Scheme displaying the synthetic strategy used to prepare PEDOT (control) and PEDOT-peptide bilayered films (a and b, respectively). The strategy involved a two-step process: (1) deposition of the internal PEDOT layer onto the AISI steel electrode; and (2) deposition of PEDOT (a) or PEDOT-peptide (b) onto the layer prepared in (1). It is worth noting that a and b only differ in the absence or presence of peptide in the generation medium used for step 2. After this, subsequent surface functionalization with fibrin and application as selective bioactive surface are also displayed. RE, WE and CE refer to the reference electrode, working electrode and counter electrode, respectively.

Figure 2. Topographic (3D) and heigh (2D) AFM images of (a) PEDOT, (b) PEDOT-CREKA and (c) PEDOT-CR(*N*Me)EKA.

Figure 3. High-resolution XPS spectra in the N 1s region for (a) PEDOT, (b) PEDOT-CREKA and (c) PEDOT-CR(*N*Me)EKA. Peaks from deconvolution are also displayed.

Figure 4. Initial control voltammogram (a), voltammogram after five consecutive oxidation-reduction cycles (b) and variation of the LEA (Eq 1) against the number of redox cycles (c) in 0.1 M PBS (pH= 7.4) of PEDOT, PEDOT-CREKA and PEDOT-CR(*N*Me)EKA. Initial and final potentials: -0.40 V; reversal potential: 0.80 V. Scan rate: 50 mV/s.

Figure 5. (a) THR-catalyzed polymerization of Fg monitored by DLS. Polymerization was initiated by adding THR (0.01 U/mL) to a Fg (0.4 mg/mL) filtered aqueous solution (5 mM $CaCl_2$ and 76 mM NaCl). These experimental conditions were taken from reference [30]. Polymer formation was measured through the the effective diameter (D_{eff} , in nm) as a function of time (in min). CREKA (b) and CR(*N*Me)EKA

(c) were added (0.1 mg/mL) to the same Fg solutions with and without THR to evaluate the influence of the peptide in the polymerization process. In all cases data correspond to the average of at least three independent experiments.

Figure 6. Low and high resolution SEM images of fibrin particles adsorbed onto (a) PEDOT-CREKA and (b) PEDOT-CR(*N*Me)EKA. White boxes in (a) and (b) indicate the magnified regions.

Figure 7. Optical images of eosin stained fibrin adsorbed on (a) steel, (b) PEDOT, (c) PEDOT-CREKA and (d) PEDOT-CR(*N*Me)EKA.

Figure 8. (a) Bode plots for all stainless steel electrodes coated with PEDOT-peptide without and with fibrin adsorbed at the surface. (b) Electrical equivalent circuits for bare steel, steel coated with PEDOT, PEDOT-CREKA and PEDOT-CR(*N*Me)EKA without and with fibrin adsorbed at the surface (see Table 3).

Figure 9. (a) Percentage of MCF-7 cells attached to different surfaces: bare steel, PEDOT, biocomposites, and biocomposites coated with fibrin. In all cases data correspond to the average of five independent assays ± the standard deviation. Asterisk marks (*) and (***) represent significant difference among the samples at $p < 0.05$ and $p < 0.001$, respectively. SEM micrographs of MCF-7 cells onto PEDOT-CR(*N*Me)EKA films (b) without and (c) with adsorbed fibrin at the surface. (d) Comparison of the percentage of normal (PNT2) and metastatic (PC3) prostate epithelial cells attached to different surfaces. The description of both the surfaces and the marks is identical to that given for (a). SEM micrographs of PC-3 cells onto (e) PEDOT-CR(*N*Me)EKA and (f) and PEDOT films. Scale bar: 20 μm.

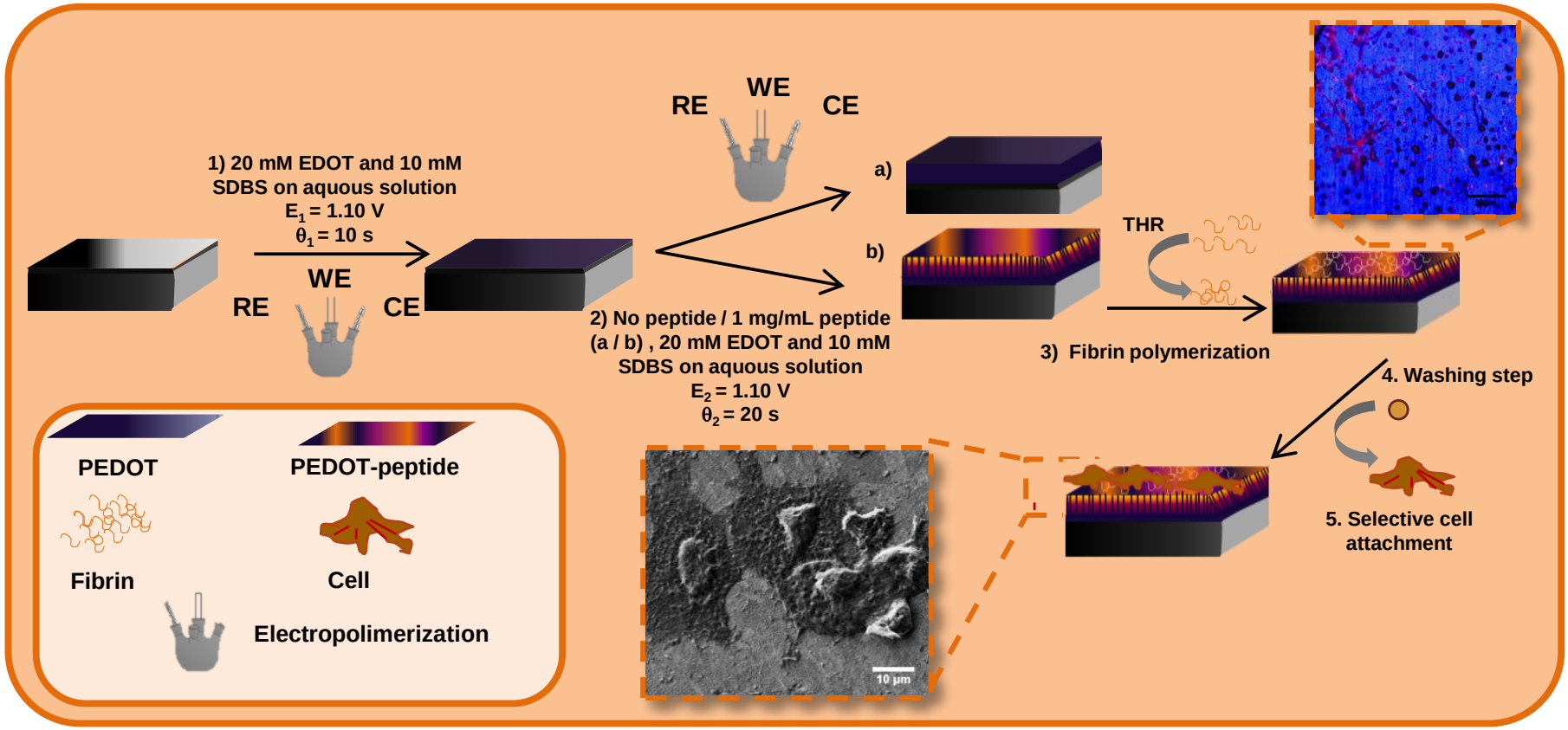
1) 20 mM EDOT and 10 mM
SDBS on aquous solution
E_1 = 1.10 V
θ_1 = 10 s
RE
WE
CE
2) No peptide / 1 mg/mL peptide
(a / b) , 20 mM EDOT and 10 mM
SDBS on aquous solution
E_2 = 1.10 V
θ_2 = 20 s
a)
b)
THR
3) Fibrin polymerization
4. Washing step
5. Selective cell
attachment
PEDOT
PEDOT-peptide
Fibrin
Cell
Electropolimerization
10 µm

Figure 1

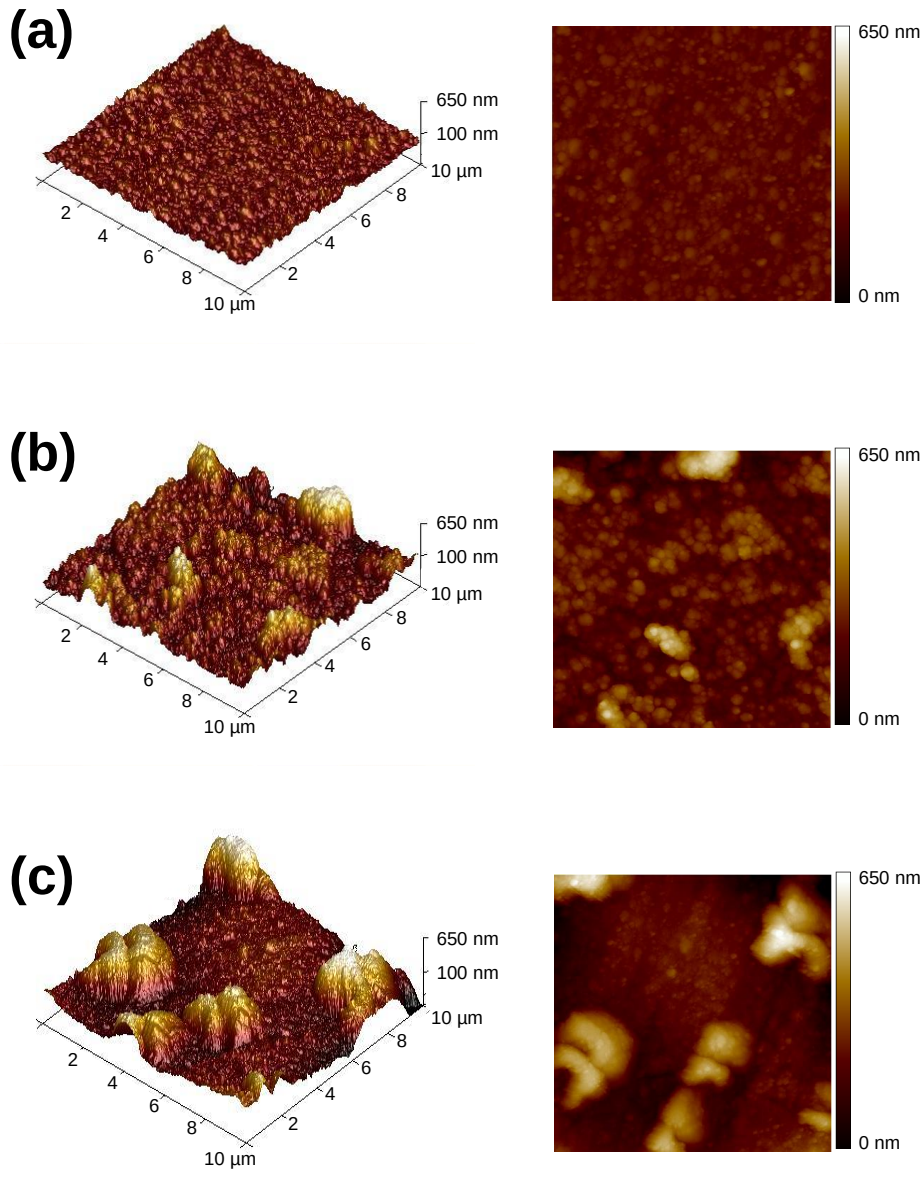
(a)
650 nm
100 nm
10 µm
2
4
6
8
10 µm
650 nm
0 nm
(b)
650 nm
100 nm
10 µm
2
4
6
8
10 µm
650 nm
0 nm
(c)
650 nm
100 nm
10 µm
2
4
6
8
10 µm
650 nm
0 nm

Figure 2

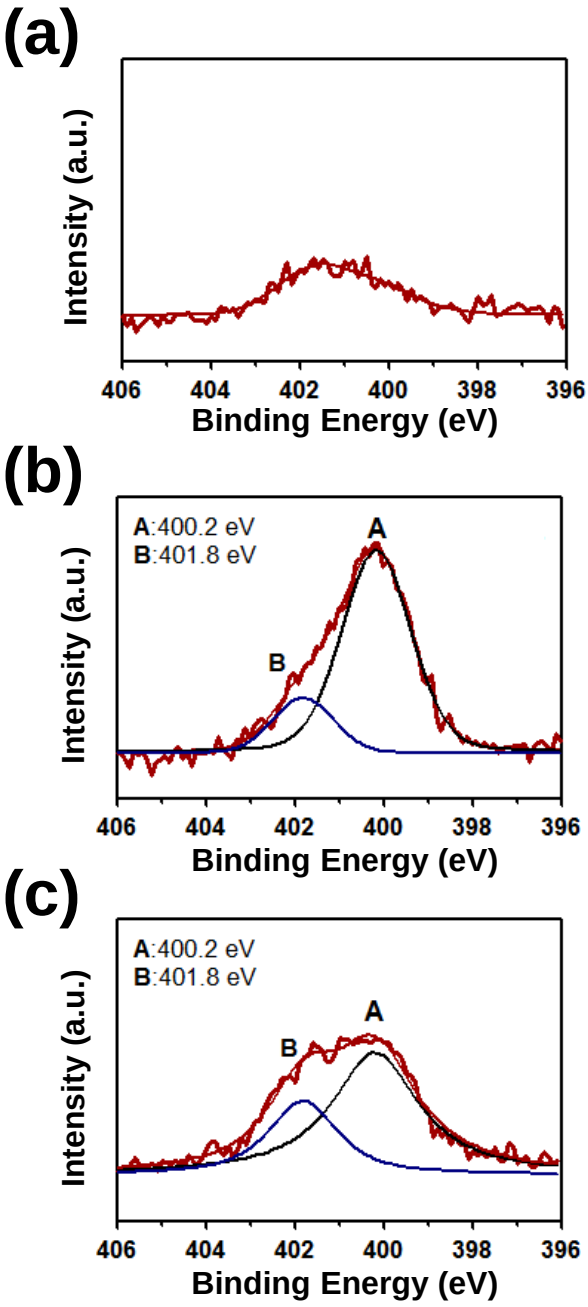
(a)
Intensity (a.u.)
406
404
402
400
398
396
Binding Energy (eV)
(b)
A:400.2 eV
B:401.8 eV
A
B
Intensity (a.u.)
406
404
402
400
398
396
Binding Energy (eV)
(c)
A:400.2 eV
B:401.8 eV
A
B
Intensity (a.u.)
406
404
402
400
398
396
Binding Energy (eV)

Figure 3

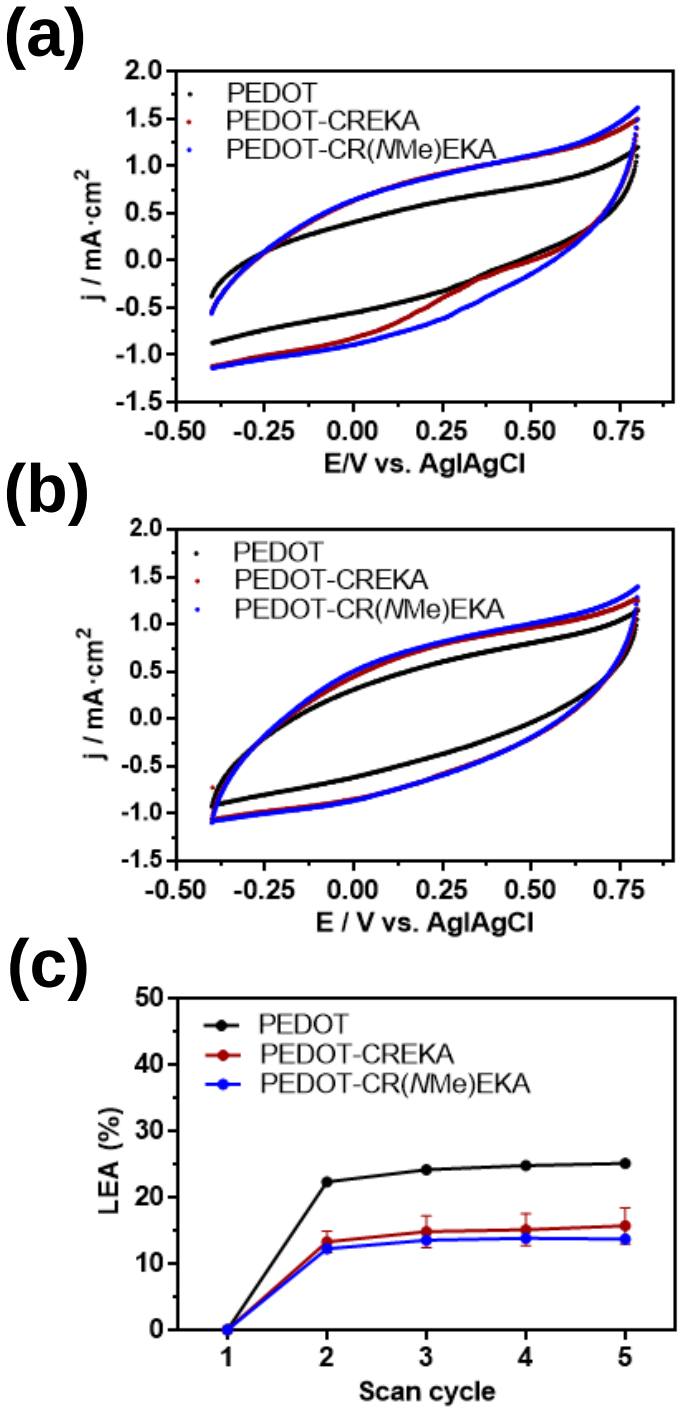
(a)
PEDOT
PEDOT-CREKA
PEDOT-CR(NMe)EKA
j / mA·cm²
E/V vs. AgIAgCl
(b)
PEDOT
PEDOT-CREKA
PEDOT-CR(NMe)EKA
j / mA·cm²
E / V vs. AgIAgCl
(c)
PEDOT
PEDOT-CREKA
PEDOT-CR(NMe)EKA
LEA (%)
Scan cycle

Figure 4

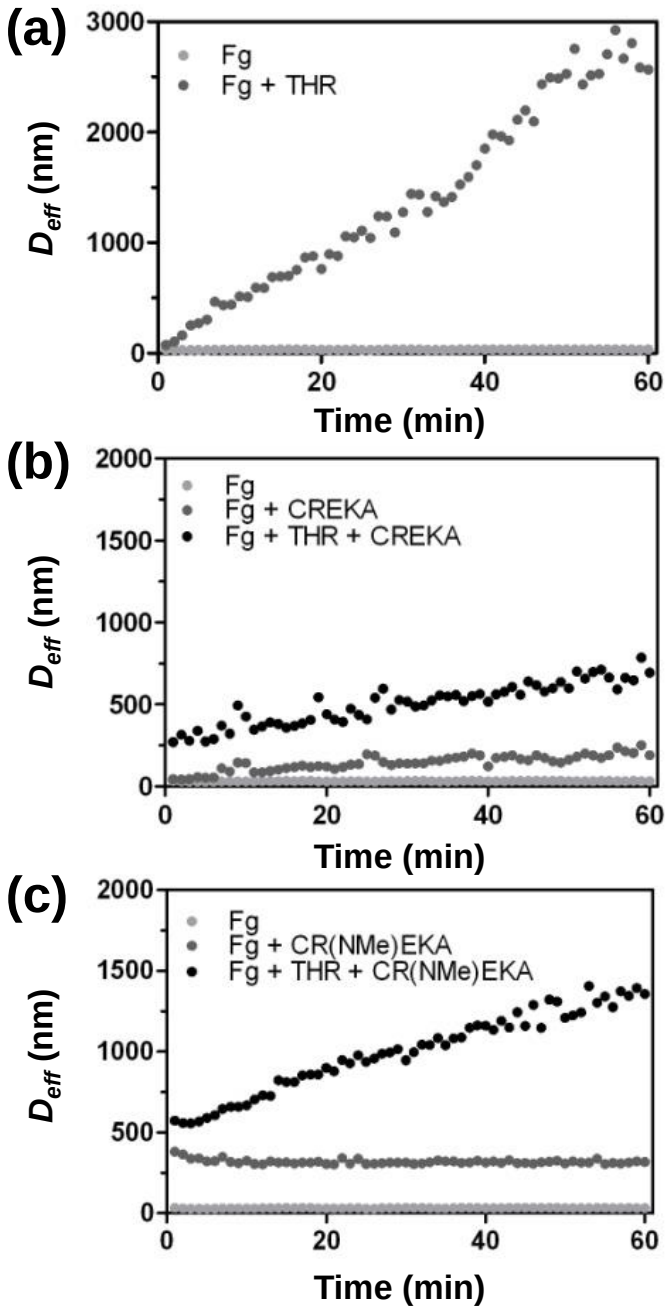
(a)
3000
2000
1000
0
Fg
Fg + THR
D_{eff} (nm)
0
20
40
60
Time (min)
(b)
2000
1500
1000
500
0
Fg
Fg + CREKA
Fg + THR + CREKA
D_{eff} (nm)
0
20
40
60
Time (min)
(c)
2000
1500
1000
500
0
Fg
Fg + CR(NMe)EKA
Fg + THR + CR(NMe)EKA
D_{eff} (nm)
0
20
40
60
Time (min)

Figure 5

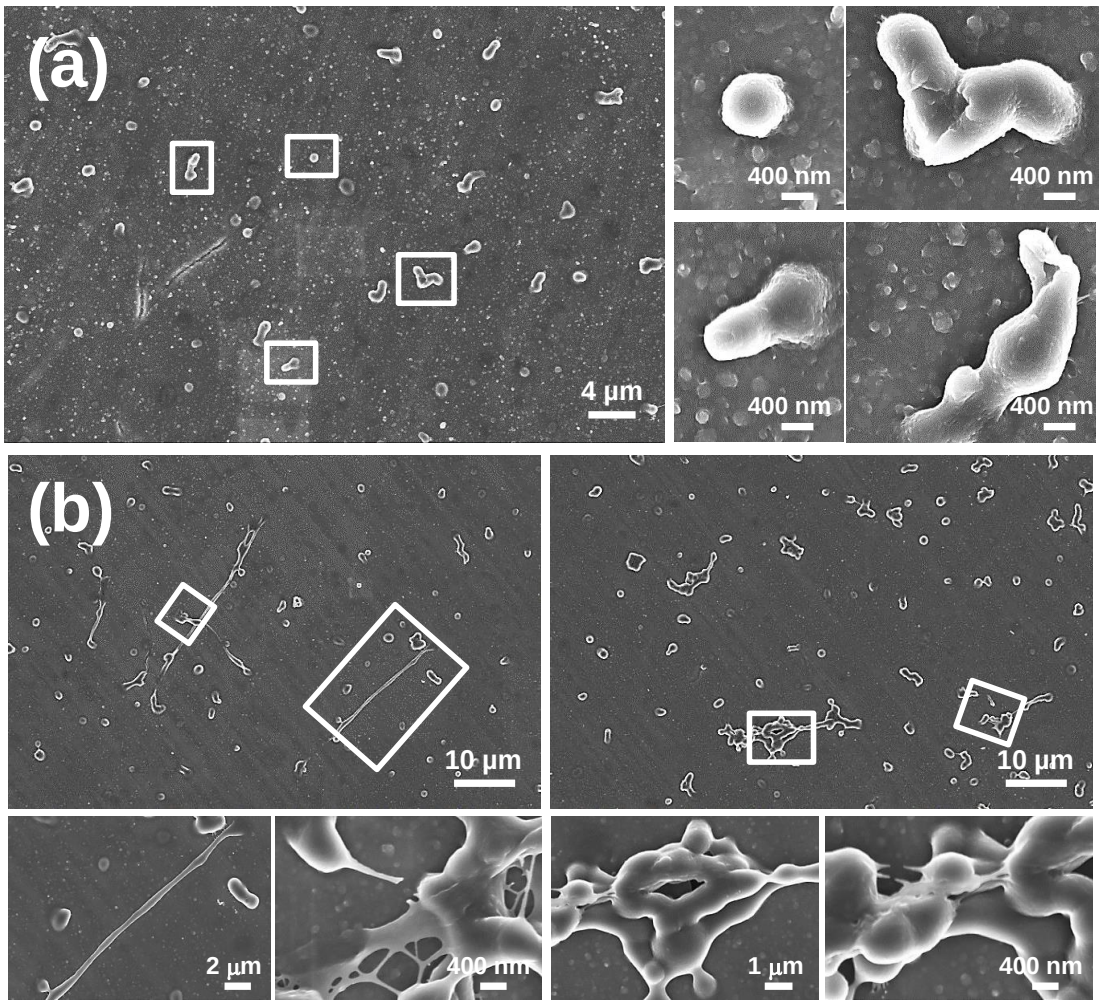

Figure 6

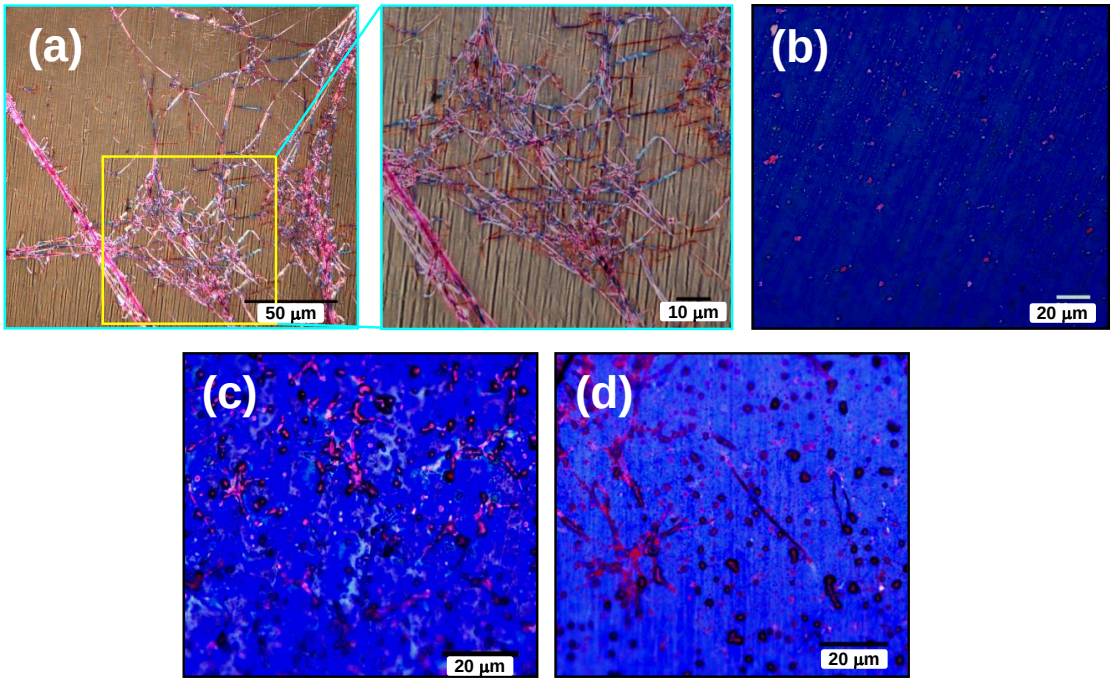

Figure 7

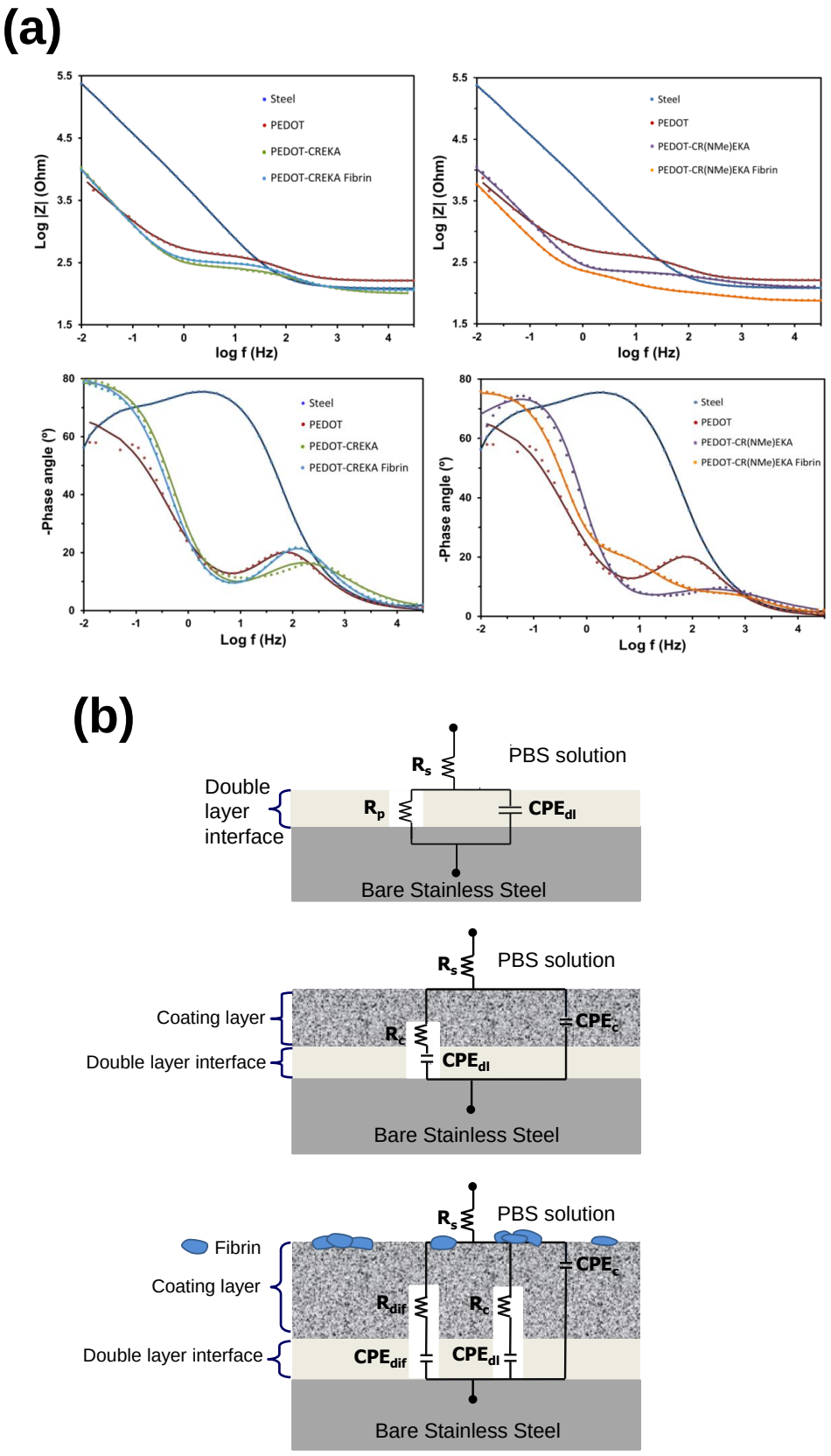
(a)
Steel
PEDOT
PEDOT-CREKA
PEDOT-CREKA Fibrin
PEDOT-CR(NMe)EKA
PEDOT-CR(NMe)EKA Fibrin
Log |Z| (Ohm)
log f (Hz)
-Phase angle (°)
Log f (Hz)
(b)
PBS solution
Double layer interface
Bare Stainless Steel
Coating layer
Fibrin

Figure 8

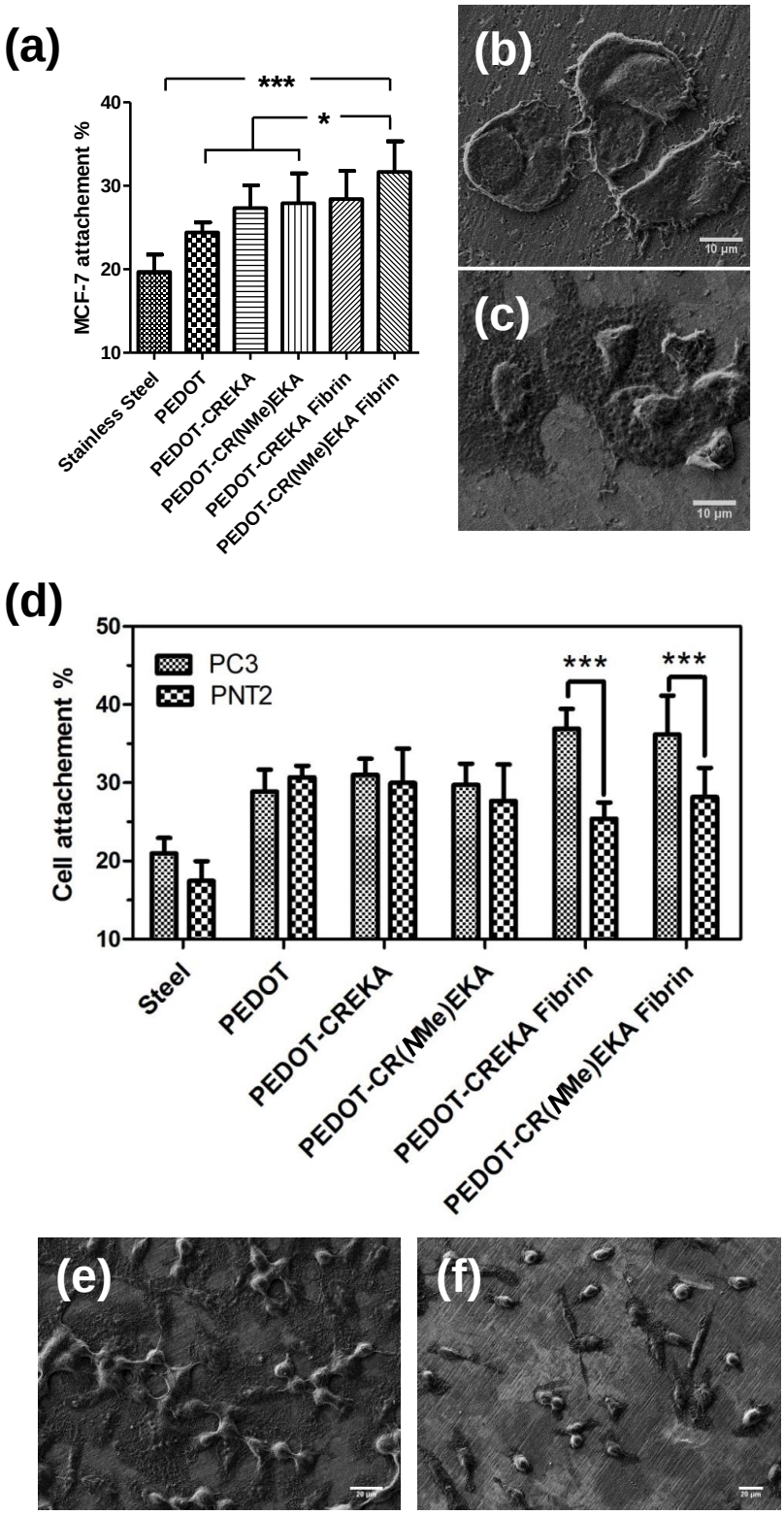
(a)
***
*
MCF-7 attachement %
40
30
20
10
Stainless Steel
PEDOT
PEDOT-CREKA
PEDOT-CR(NMe)EKA
PEDOT-CREKA Fibrin
PEDOT-CR(NMe)EKA Fibrin
(b)
10 µm
(c)
10 µm
(d)
PC3
PNT2
Cell attachement %
50
40
30
20
10
***
***
Steel
PEDOT
PEDOT-CREKA
PEDOT-CR(NMe)EKA
PEDOT-CREKA Fibrin
PEDOT-CR(NMe)EKA Fibrin
(e)
(f)

Figure 9

Supporting Information

for *Macromol. Biosci.*, DOI: 10.1002/mabi.2013#####

Fibrin Association at Hybrid Biointerfaces Made of Clot-Binding Peptides and Polythiophene

Anna Puiggalí,[1,2] Luis J. del Valle,[1,2,*] Elaine Armelin[1,2] and Carlos Alemán[1,2,*]

Experimental Methods

***Materials*.** 3,4-ethylenedioxythiophene (EDOT) monomer and dodecylbenzene sulfonate (SDBS) were purchased from Aldrich and used as received without further purification. CR(*N*Me)EKA and CREKA peptides with > 98% of HPLC purity was purchased from Biomatik (Toronto, ON). Ultrapure milliQ water was used to prepare all the aqueous solutions. Fibrinogen from human plasma (50-70% protein; ≥ 80% of protein is clottable) was purchased from Sigma (F3879). Cell lines MCF-7 (epithelial cells from human breast adenocarcinoma), PNT2 (normal prostate epithelium immortalized with SV40), and PC-3 (epithelial cells from human prostate adenocarcinoma) were obtained from ECACC (European Collection of Cell Culture, UK). Culture media were purchased from BD Gibco (Franklin Lakes, NJ, USA.

Synthesis. Anodic polymerization and electrochemical assays were performed with an Autolab PGSTAT302N equipped with the ECD module (Ecochimie, the Netherlands) using a three-electrode compartment cell under nitrogen atmosphere (99.995% pure) at room temperature. Steel AISI 316 sheets of 0.5 and 1 cm^2 in area

were used as working and counter electrode, respectively. The reference electrode was an Ag|AgCl electrode containing a KCl saturated aqueous solution.

PEDOT-CR(*N*Me)EKA and PEDOT-CREKA films were prepared by chronoamperometry using an aqueous medium pH = 10.3 (adjusted with 1 M NaOH) and a constant potential of 1.10 V, which has been identified as the optimum potential for the polymerization of EDOT in water.[1] A two-step process was used. First, steel electrode was coated with a layer of PEDOT. For this purpose, the anodic compartment of the cell was filled with 20 mL of a 20 mM EDOT aqueous solution containing 10 mM SDBS as supporting electrolyte, while the cathodic compartment was filled 10 mL of the same electrolyte solution. The polymerization time used for the electrodeposition of this PEDOT coating layer was of θ= 10 s. After this, a second layer of PEDOT-CR(*N*Me)EKA or PEDOT-CREKA was electrodeposited onto the surface of the PEDOT coating layer. This was achieved by filling the anodic compartment with a generation solution identical to that described above for the internal PEDOT layer but containing 1 mg/mL of CR(*N*Me)EKA or CREKA peptide. The applied potential and the polymerization time employed for the preparation of the second layer were 1.10 V and θ= 20 s, respectively. It should be remarked that the biocomposite layer was deposited onto the internal PEDOT layer immediately after the generation of the latter. This represents an important difference with respect to our previous work,[2] in which the PEDOT-CREKA layer was deposited after dry during several hours the internal PEDOT layer.

PEDOT films used as control were prepared employing the same experimental conditions that for PEDOT-CREKA and PEDOT-CR(*N*Me)EKA biocomposites but without the peptide addition in the second layer (*i.e.* two PEDOT layers prepared using polymerization times of 10 s and 20 s).

Contact profilometry. Film thickness measurements were carried out using a Dektak 150 stylus profilometer (Veeco, Plainview, NY). Scratches were intentionally provoked on the film surface and the average thickness was determined from, at least, nine measurements for each condition. Imaging of the films was conducted using the following optimized settings: tip radius= 12.5 μm; stylus force= 3 mg; scan length= 2 μm; speed= 2 nm/s.

Atomic Force Microscopy (AFM). AFM was conducted to obtain topographic images of the films surface using silicon TAP 150-G probe (Budget Sensors, Bulgaria) with a frequency of 150 kHz and a force constant of 5 N/m. Images were obtained with a AFM Dimension microscope using a NanoScope IV controller under ambient conditions in tapping mode. The row scanning frequency was set between 0.6 and 0.8 Hz. The Root Mean Square roughness (Rq), which is the average height deviation taken from the mean data plane, was determined using the statistical application of the NanoScope Analysis software (1.20, Veeco). AFM measurements were performed on various parts of the films, which produced reproducible images similar to those displayed in this work. The scan window size was $10 \times 10\ \mu m^2$.

X-ray photoelectron spectroscopy (XPS). XPS analyses were performed in a SPECS system equipped with a high-intensity twin-anode X-ray source XR50 of Mg/Al (1253 eV/1487 eV) operating at 150 W, placed perpendicular to the analyzer axis, and using a Phoibos 150 MCD-9 XP detector. The X-ray spot size was 650 mm. The pass energy was set to 25 and 0.1 eV for the survey and the narrow scans, respectively. Charge compensation was achieved with a combination of electron and argon ion flood guns. The energy and emission current of the electrons were 4 eV and 0.35 mA, respectively. For the argon gun, the energy and the emission current were 0 eV and 0.1 mA, respectively. The spectra were recorded with a pass energy of 25 eV in 0.1 eV steps at a

pressure below 6×10^{-9} mbar. These standard conditions of charge compensation resulted in a negative but perfectly uniform static charge. The C 1s peak was used as an internal reference with a binding energy of 284.8 eV. High-resolution XPS spectra were acquired by Gaussian–Lorentzian curve fitting after S-shape background subtraction. The surface composition was determined using the manufacturer's sensitivity factors.

Cyclic voltammetry (CV). CV studies were run to assess the electrochemical behavior of the biocomposites. Hence, the ability to exchange charge reversibly (*i.e.* electroactivity) and the electrochemical stability *(i.e.* electrostability) were determined using a 0.1 M phosphate buffer saline solution (PBS; pH= 7.4 adjusted with NaOH). The initial and final potentials were -0.40 V, whereas a reversal potential of 0.80 V was considered. The scan rate was 50 mV/s in all cases.

The electroactivity increases with the similarity between the anodic and cathodic areas of the first control voltammogram. The electrochemical stability (*i.e.* loss of electroactivity, LEA), which decreases with the oxidation and reduction areas of consecutive control voltammograms, was determined using the following expression:

$$LEA = \frac{\Delta Q}{Q_i}100 \qquad (1)$$

where ΔQ is the difference of voltammetric charge between the first cycle and the last cycle and Q_i is the voltammetric charge corresponding to the second cycle. In this work all values of *LEA* were referred to five consecutive oxidation-reduction cycles.

Dynamic light scattering (DLS). Real-time monitoring of fibrin polymerization in presence and absence of peptide at 37 ºC was conducted by DLS following the increment of the particle effective diameter. All buffers and fibrinogen (Fg) samples were filtered (0.22 μm centrifugal filter) prior to use. Final concentrations of Fg and

thrombin (THR) were 0.4 mg/mL and 0.01 U/mL, respectively, in aqueous solution containing 5 mM $CaCl_2$ and 76 mM NaCl. Data were collected every minute. Measurements were performed using a NanoBrook Omni Zeta Potential Analyzer from Brookheaven Instruments Corporation.

Electrochemical impedance spectroscopy (EIS). Impedance spectroscopy was performed using a conventional three-electrode cell and AUTOLAB-302N potentiostat/galvanostat operating between the frequency range of 100kHz-10 mHz and 10 mV of amplitude for the sinusoidal voltage. All experiments were performed with films electrochemically deposited on stainless steel substrates (AISI 316L with $1cm^2$ of area) and immersed in phosphate buffer saline (PBS, pH 7.4), at room temperature. Stainless steel electrodes were used as working and counter-electrodes, whereas Ag|AgCl saturated (KCl 3M) was employed as reference electrode. After data collection, EIS results were then processed and fitted to an electrical equivalent circuit (EEC).

Protein Adsorption. Analyses to examine the adsorption of proteins onto the surface of PEDOT, PEDOT-CREKA and PEDOT-CR(*N*Me)EKA films were performed using fibrin and bovine serum albumin (BSA, Fraction V). BSA, which is a globular plasma protein, was used as a control to study the selectivity of the examined surfaces.

PEDOT and PEDOT-peptide films were placed on a 24-well plate heated at 37 ºC. Meanwhile, fibrin precursors, Fg (0.4 mg/mL) and THR (0.01 U/mL) were heated to the same temperature (solutions previously filtered). Fg and THR solutions were deposited onto the film surface using a 1:1 ratio. After 60 min with slight agitation (80 rpm) the film was rinsed in 0.1 M PBS to remove residues and non-specifically bound fibrin**.** The same procedure was used to adsorb BSA, the only difference being the protein concentration in the solution (0.4 mg/mL).

Detection of adsorbed proteins: Bradford method. Adsorbed fibrin and BSA were removed from the films surfaces by adding 0.2 mL of 0.1 M PBS with nonyl phenoxypolyethoxyethanol (NP-40) surfactant (0.5% v/v) and orbital shaking at 50 rpm during 30 min and 37ºC. In order to avoid interferences between the NP40 surfactant and the Bradford reagent, the former was eliminated by precipitating the fibrin with 20 µL of trichloroacetic acid. Then, the precipitate-containing solution was centrifuged for 15 min at 12000 rpm. The solid (fibrin or BSA) was washed with cold acetone and maintained at 4 ºC for 1 hour. After this, the solid was centrifuged again during 15 min at 12000 rpm. The protein was dried under vacuum and, finally, dissolved in 0.1 M PBS for Bradford assay.

Standard curves were carried out using protein dilutions, which were prepared using buffer solution with concentrations of protein ranging from 0.05 to 1.00 mg/mL. Next, 5 µL of protein standards and samples were added to a 96-well plate, blank wells were filled with 5µL of buffer. After this, Bradford reagent (250 µL) was added and, subsequently, mixed on a shaker for 30 s. Samples were incubated at room temperature for 15 min. Finally, the absorbance was measured at 595 nm.

Scanning electron microscopy (SEM). SEM micrographs were obtained using a Focussed Ion Beam Zeiss Neon 40 scanning electron microscope operating at 10 kV. Samples were mounted on a double-side adhesive carbon disc and sputter-coated with a thin layer of carbon to prevent sample charging problems. The projected area and best-fit ellipse aspect ratio of fibrin structures were calculated using ImageJ software.

Optical microscopy. To evaluate the THR-catalysed fibrin particles, samples were washed three times with milliQ water to avoid unspecific bindings. After this, fibrin particles were fixed onto the surface with 300 µL of 2.5% paraformaldehyde in PBS during 30 min at 4 ºC. Then, samples were progressively dehydrated using alcohols of

30º, 40º, 50º, 70º, 95º, and 100º for 15 min each at 4 ºC. Samples were stained with eosin for 30 min. Eosin is a fluorescent acidic compound that binds positively charged molecules (*i.e.* the isoelectric point of Fg is 5.5, increases to ~6.3 after clipping of polar residues in the clotting response by THR). Finally, samples were washed three times again with milliQ water and left on vacuum overnight.

Wettability. Contact angle (CA) measurements were conducted using the water drop method. 0.5 µL of milliQ water drops were deposited onto the surface of the films and recorded after stabilization with the equipment OCA 15EC (DataPhysics Instruments GmbH, Filderstadt). The SCA20 software was used to measure the CA, which is shown here as the average of at least 10 measures for each condition.

Cell capture assays. Substrates were placed into a 24-well plate, and 1 mL of cell MCF-7 (breast cancer cell line), PNT2 (normal prostate epithelial cell line) or PC-3 (cancer prostate epithelial cell line) suspension (10^5 cells/mL) was loaded. After incubation for 30 min at 37 ºC, 5% CO_2 with slight agitation (80 rpm), the substrates were washed with PBS, located in a new 24-well plate and incubated for 24 hours. The percentage of cells adhered in the substrate with respect to the amount deposited into the well was determined using the MTT [3-(4,5-dimethylthiazol-2-yl)-2,5-diphenyltetrazolium] method. Cell capture assays were repeated two times with at least 4 replicas, showing similar results in all cases.

For the observation of the cell morphology in the scanning electronic microscope, all samples were previously coated with a carbon layer of 6−10 nm thickness using a K950X Turbo Evaporator to prevent sample charging problems. Before the carbon coating, samples covered with cells were fixed in a 2.5% formaldehyde PBS solution (pH = 7.2) overnight at 4 °C. Then, they were dehydrated by washing in an alcohol

battery (30°; 50°; 70°; 90°; 95°; and 100°) at 4 °C for 15 min per wash. Finally, samples were air-dried and sputter-coated with carbon.

(1) Aradilla, D.; Estrany, F.; Azambuja, D. S.; Casas, M. T.; Puiggalí, J.; Ferreira, C. A.; Alemán, C. Conducting Poly(3,4-ethylenedioxythiophene)-Montmorillonite Exfoliated Nanocomposites. *Eur. Polym. J.* **2010**, *46*, 977-983.
(2) Fabregat, G.; Teixeira-Dias, B.; del Valle, L. J.; Armelin, E.; Estrany, F.; Alemán, C.; Incorporation of a Clot-Binding Peptide into Polythiophene: Properties of Composites for Biomedical Applications. *Appl. Mater. Interfaces* **2014**, *6*, 11940-11954.

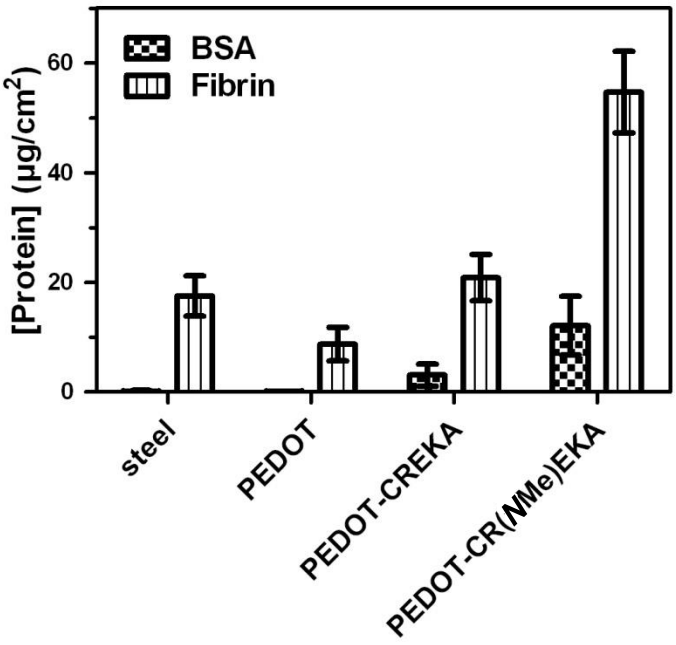

Figure S1. Adsorption of fibrin and BSA onto the surface of PEDOT and PEDOT-peptide films. Four samples were analysed for each group. Bars represent the mean ± standard deviation.

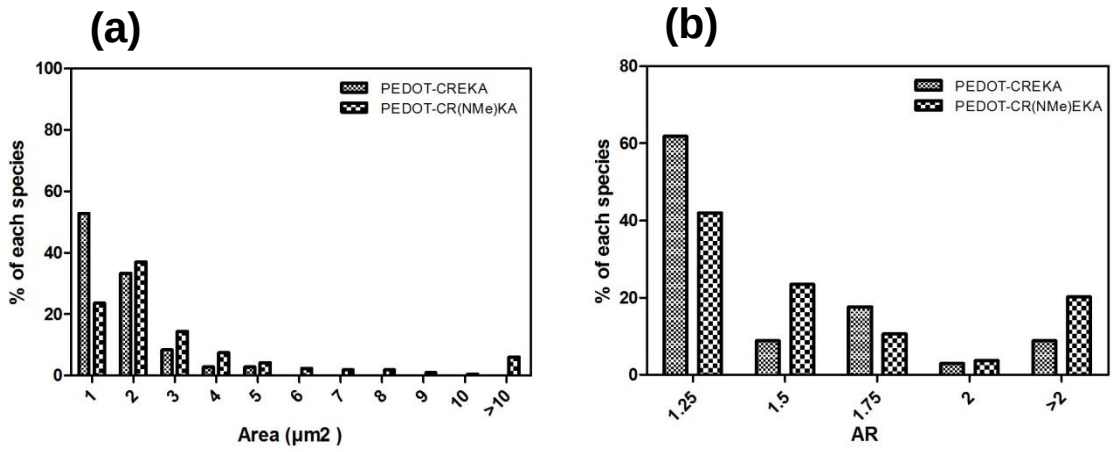

Figure S2. Quantitative assessment of the fibrin particles adsorbed onto PEDOT-CREKA and PEDOT-CR(*N*Me)EKA surfaces. Histogram showing the percentage of (a) the area and (b) the aspect ratio (AR) of the adsorbed fibrin structures after 60 min of the addition of THR and Fg.

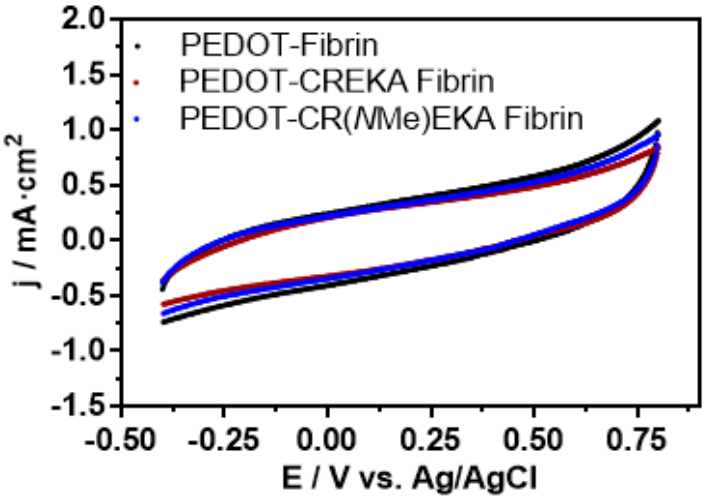

Figure S3. Control voltammograms in 0.1 M PBS (pH= 7.4) of fibrin-coated PEDOT, PEDOT-CREKA and PEDOT-CR(*N*Me)EKA films. Initial and final potentials: -0.40 V; reversal potential: 0.80 V. Scan rate: 50 mV/s.

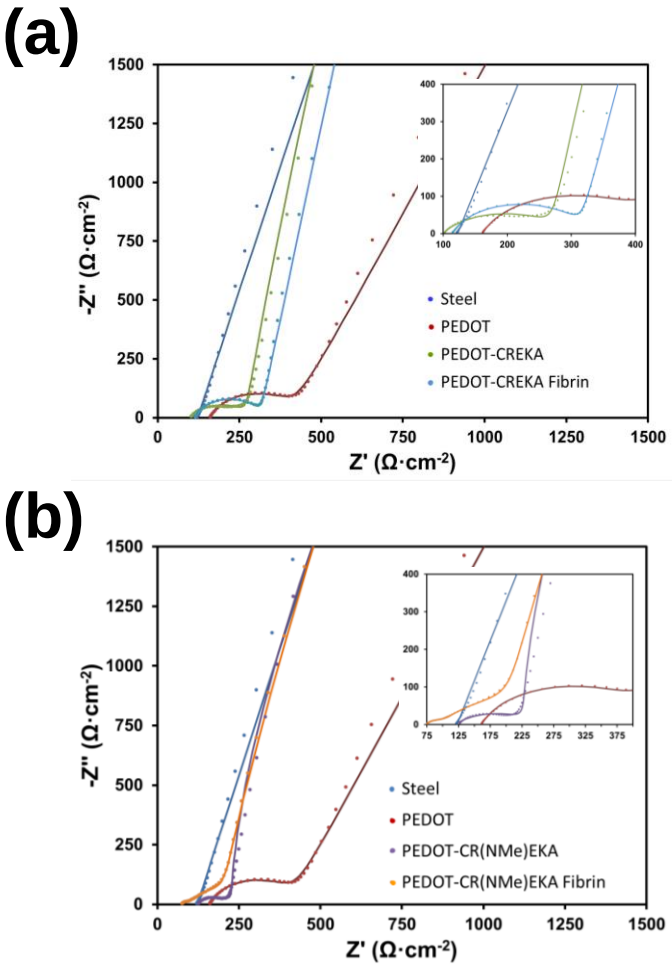

Figure S4. Nyquist plots for all stainless steel electrodes coated with (a) PEDOT-CREKA and (b) PEDOT-CR(*N*Me)EKA without and with fibrin adsorbed at the surface.